CZECH TECHNICAL UNIVERSITY IN PRAGUE

FACULTY OF MECHANICAL ENGINEERING

Department of production machines

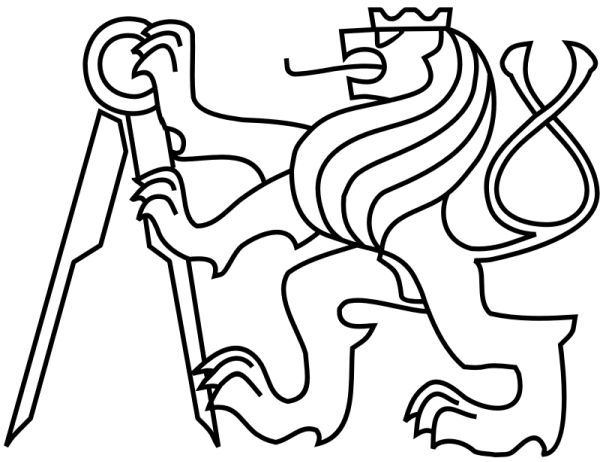

Master‘s thesis

Experimental Determination of Thermal Resistance across Linear Guideways

2015 **Bc. Petr Morávek**

CZECH TECHNICAL UNIVERSITY IN PRAGUE
Faculty of Mechanical Engineering
Department of production machines

Statement

I declare that my thesis was developed independently and that all used information sources are stated in enclosed list in accordance with the Guidelines of adhering to ethical principles in the preparation of undergraduate theses, issued by the Czech Technical University in Prague on 1/7 2009.

I do not have a relevant reason against the use of this school work in accordance with § 60 of the Act no.121 / 2000 Sb., on copyright, rights related to copyright and amending some laws (Copyright Act).

In Prague on 12/6 2015 ……..…….

signature

Acknowledgement

I would like to express my gratitude to the supervisor of my thesis, Otakar Horejš, PhD, for guidance of my thesis and factual comments. I am also very grateful to Peter Kohút, PhD, for his help with the experimental part, and to Jaroslav Šindler for his help with the evaluation of results. Least but not last, I would like to thank to the SCHNEEBERGER company, especially to ing. Roland Wolk, for supporting this thesis with their linear guideways.

CZECH TECHNICAL UNIVERSITY IN PRAGUE
Faculty of Mechanical Engineering
Department of production machines

Annotation

Author :	Petr Morávek
Title of master thesis :	Experimental Determination of Thermal Resistance Across Linear Guideways
Extent :	77 pages, 54 figures, 10 tables
Academic year:	2014/2015
Department :	Ú12135 – Department of Production Machines
Supervisor :	Otakar Horejš PhD
Consultant :	Peter Kohút, PhD, Jaroslav Šindler
Submitter of the Theme :	CTU – Faculty of Mechanical Engineering
Application :	FEM models describing thermo-mechanical behavior of machine tool
Key words :	linear guideway, thermal resistance
Annotation:	This thesis deals with experimental determination of thermal resistances across linear guideways. The thermal resistances are determined for linear guideways differing in size, type of rolling elements and preload. From the results influence of these parameters on thermal resistance of linear guideways is investigated. Usage of obtained data in thermal FE modeling of linear guideways is stated.

Anotace

Jméno autora :	Petr Morávek
Název DP :	Experimentální zjišťování tepelných odporů lineárních vedení
Rozsah práce :	77 stran, 54 obrázků, 10 tabulek
Šk. rok vyhotovení:	2014/2015
Ústav :	Výrobní stroje a zařízení
Vedoucí BP :	Ing. Otakar Horejš, Ph.D
Konzultant :	Ing. Petr Kohút, Ph.D., Jaroslav Šindler
Zadavatel tématu :	ČVUT v Praze – Fakulta strojní
Využití :	MKP modely popisující teplotně mechanické chování obráběcích strojů
Klíčová slova :	lineární vedení, tepelný odpor
Anotace:	Diplomová práce se zabývá experimentálním stanovením tepelných odporů lineárních vedení. Tepelné odpory jsou určeny pro valivé lineární vedení lišící se velikostí, typem valivých elementů a velikostí předpětí. Z výsledků je stanoven vliv těchto parametrů na tepelný odpor lineárního vedení a dále jsou uvedeny možnosti použití výsledků při modelování lineárních vedení v MKP.

Content

Nomenclature

Symbol	Quantity	Unit
A	Area	m^2
C	Coverage factor	1
C	Specific heat	J/(kg·K)
C_{100}	Dynamic loading capacity	N
dT	Temperature difference between the top and the bottom of the carriage	°C
E	Young's modulus of elasticity	N/m^2
E_b	Upper limit of the emissive power	W/m^2
E_p	Emissive power	W/m^2
F_{V1}	Preload of class V1	N
F_{V3}	Preload of class V3	N
FD	Flatness deviation	m
H	Convection heat transfer coefficient	$W/(m^2 \cdot K)$
H_c	Surface hardness	Pa
I	Electric current	A
$[I]$	Identity matrix	1
k	Thermal conductivity coefficient	W/(m·K)
$[K]$	Thermal conductivity matrix	W/°C
L	Length	m
ΔL	Change in length	m
m	Absolute asperity slope	1
m'	RMS asperity slope	1
m_s	Effective value of asperity slope	1
$[M]$	Thermal inertia matrix	J/°C
P	Pressure	Pa
q	Heat rate	W

$q^{"}$	Heat flux	W/m^2
$\{Q(t)\}$	Thermal exciting vector	W
r	Radius	m
R	Electric resistance	Ω
R_a	Surface roughness	m
R_T	Thermal resistance	K/W
$R_T^{"}$	Thermal contact resistance	K/(W·m^2)
s	Parameter of surface	1
S_Y	Yield strength	Pa
t	Time	s
$\{T(t)\}$	Temperature vector	°C
T_m	Average temperature of the interface	K
T_s	Temperature of the surface	K
T_∞	Temperature of the fluid	K
T1	Temperature at the top of the carriage	°C
T2	Temperature at the bottom of the carriage	°C
T3	Temperature in the rail	°C
T4	Temperature in the rail	°C
T5	Temperature at the side of the rail	°C
T0	Ambient temperature	°C
T01	Temperature at the top of the insulation	°C
T02	Temperature at the bottom of the insulation	°C
T05	Temperature at the side of the insulation	°C
ΔT	Temperature drop	°C
u_A	Uncertainty of type A	°C
u_B	Uncertainty of type B	°C
U_M	Expanded uncertainty of measurement	°C
V	Volume	m^3
[V]	Matrix which columns are the eigenvectors normalized respect to the $[M]$	(°C·J)$^{1/2}$

$\{V_i\}$	Natural thermal modes	$(°C \cdot J)^{1/2}$
x_i	Modal coordinates	$(°C \cdot J)^{1/2}$
α	Linear coefficient of thermal expansion	K^{-1}
α_R	Coefficient of electrical resistance	K^{-1}
δ	Gap thickness	m
δ_0	Gap thickness parameter	1
ε	Emissivity	1
$[\lambda]$	Diagonal matrix which elements are eigenvalues	s^{-1}
λ_i	Eigenvalue number *i*	s^{-1}
ν	Poisson´s ratio	1
ρ	Density	kg/m^3
ρ_R	Resistivity	$\Omega \cdot m$
σ	RMS roughness	m
σ_E	Stefan-Boltzmann constant	$W/(m^2 \cdot K^4)$
σ_s	Effective value of roughness	m
$\{\phi(t)\}$	Vector of modal thermal rate	$°C \cdot J$

1 Preface

This thesis deals with the influence of linear guideways on thermo-mechanical properties of machine tools. The aim was to determine thermal resistances of linear guideways. For this purpose, an experiment was designed. Various types of rolling linear guideways were measured because this type of linear guideways is most often used in CNC machine tool design. Linear guideways differing in size, type of rolling elements and size of preload were measured and the influence of these parameters in thermal resistance was evaluated based on the obtained data. The results will mainly serve to refine FE models describing thermo-mechanical behavior of machine tools.

2 Theoretical part

As this thesis deals with experimental investigation into thermal resistances of linear guideways, in chapter 2.1 basic types of linear guideways used in machine tools are described. Short chapter 2.2 is dedicated to disruptive thermal effects influencing machine tools. Chapter 2.3 sums up principles of temperature measurement and states common types of thermometers. Chapter 2.4 describes principles of heat transfer. Chapter 2.5 then defines thermal resistance and parameters that influence its value. In chapter 2.6, mathematical models for thermal contact conductance are described and chapter 2.7 states heat transfer across some typical machine parts. Chapter 2.8 then describes experiments for thermal resistance investigation.

2.1 Linear guideways

What we understand under the term of guideways is a system of areas where the moving part is in contact with the stationary part. Guideways ensure movement on a geometrically accurate trajectory [1].

Primary distribution of linear guideways used in CNC machine tools design is stated in Fig.2.1.

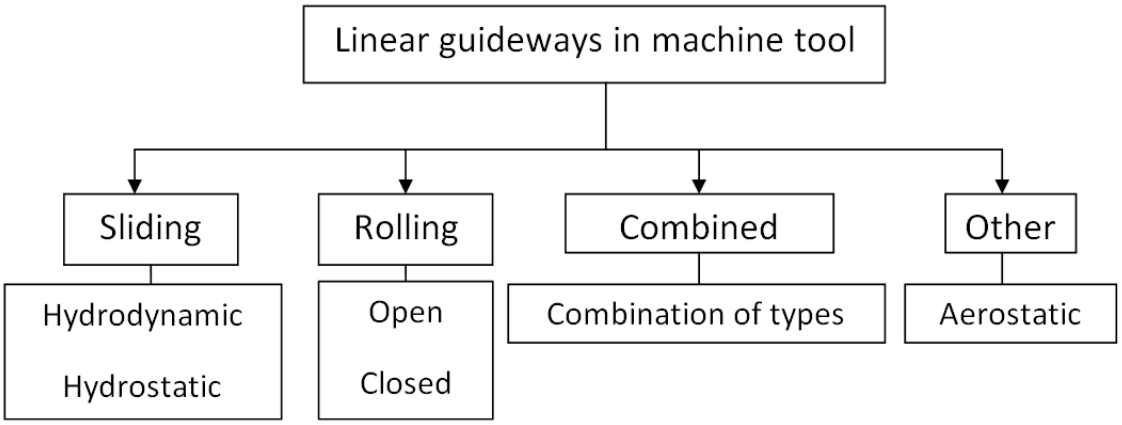

Fig. 2.1: Types of linear guideways used in machine tool design [2]

2.1.1 Sliding guideways

Sliding guideways are used in two fundamental variants based on the character of friction between sliding areas, as a hydrostatic guideway or hydrodynamic guideway [1].

The hydrodynamic guideway has its name after the fact that oil between the guideway parts creates lubricating film only when it is moving and when the conditions of hydrodynamic lubricating are formed. When this type of guideway is used, jerky movements and insensitivity in positioning can occur and therefore the quality of work degrades especially at lower speeds. In order to reduce these problems, and eventually remove them, special additive oils or lining of the sliding areas with synthetic materials is used and thereby the coefficient of friction is reduced [2].

The principle of the hydrostatic guideway is based on supplying the pressure oil between the sliding areas. Thereby fluid friction is achieved. Fluid friction has very low coefficient of friction ($5 \cdot 10^{-6}$) even at low motion speeds. The hydrostatic guideway consists of several pressure pockets that are mounted to one of the sliding areas while the second sliding area is completely smooth as it is in the hydrodynamic guideway. A comparison of friction properties of hydrodynamic and hydrostatic guideway is stated in Fig. 2.2 [1].

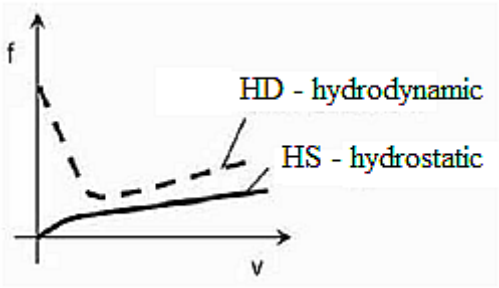

Fig 2.2: Comparison of friction properties of hydrodynamic and hydrostatic guideways [2]

This type of guideway can be further divided by the type of sliding area as shown in Fig.2.3.

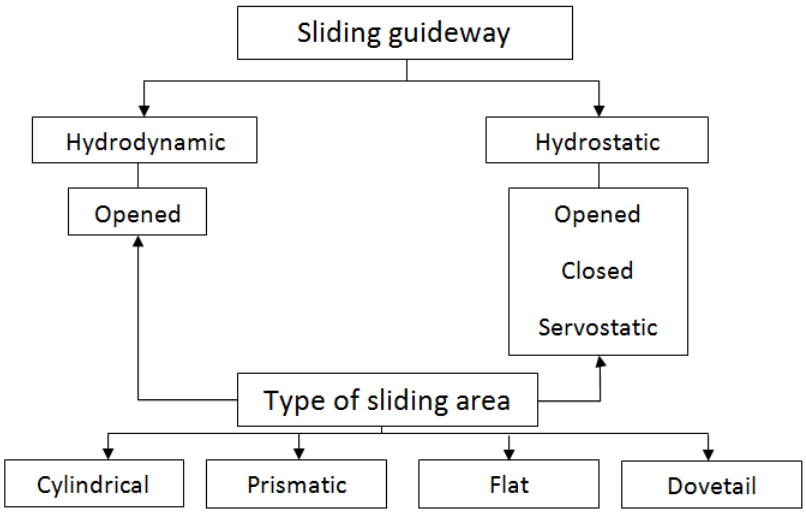

Fig. 2.3: Types of sliding guideway [1]

2.1.2 Rolling guideways

With regard to requirements of CNC machine tools the demands on perfect fluency of movement are increasing and the requirement appears to achieve the smallest variance possible in positioning. Apart from the hydrostatic guideway, these requirements can be fulfilled by rolling guideways. This type of guideway is nowadays the most widely used in the field of machine tools [2].

The benefits of this type of guideway are especially lower coefficient of friction and its minimal dependency on movement speed which results in high accuracy of positioning even at low movement speeds. Another benefit is minimal wear, leading to longer service life and the possibility of defining backlash and preload. Disadvantages include high requirements on accuracy of production resulting in higher price and also lower ability to absorb vibrations. Different types of rolling guideways are shown in Fig.2.4 [1].

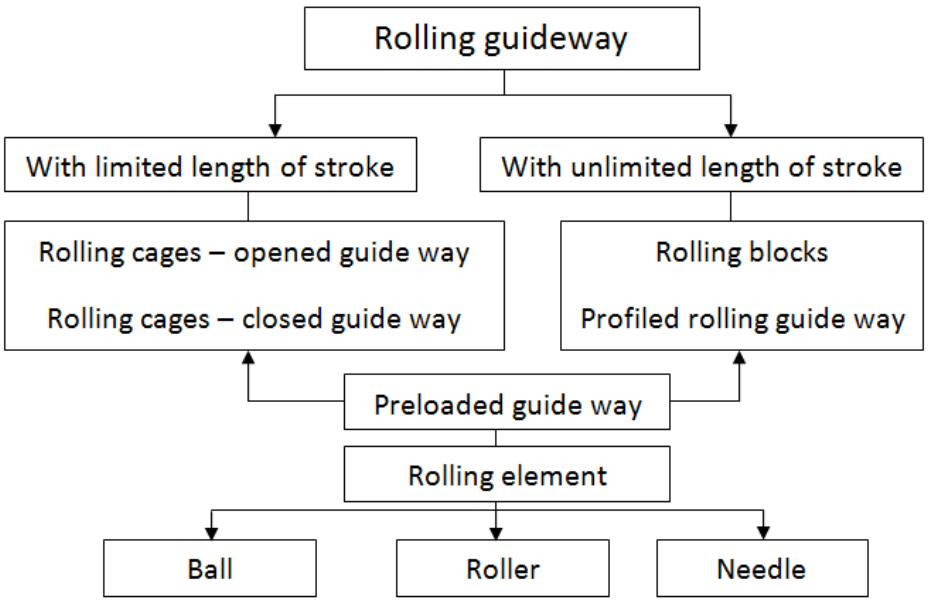

Fig. 2.4: Types of rolling guideway [2]

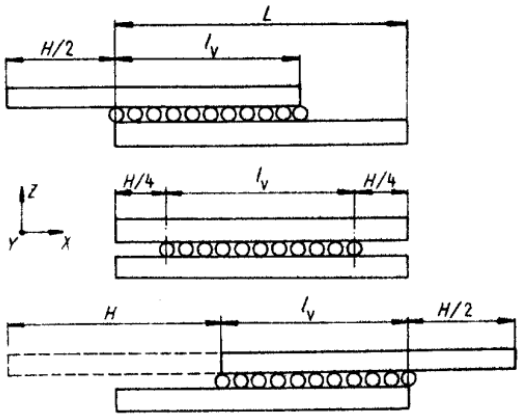

Fig. 2.5: Rolling guideway with limited length of stroke [1]

Two basic types of rolling guideways come in with limited length of stroke and with unlimited length of stroke. An example of a guideway with limited length of stroke is shown in Fig. 2.5. The stroke of the moving part is in limited this case because the cage with rolling elements executes stroke that is equal to the half of a working stroke. This type of guideway is most often designed as open. This means it intercepts only axial force effects. Closed guideways are always preloaded and have limited ability to transfer random load [2].

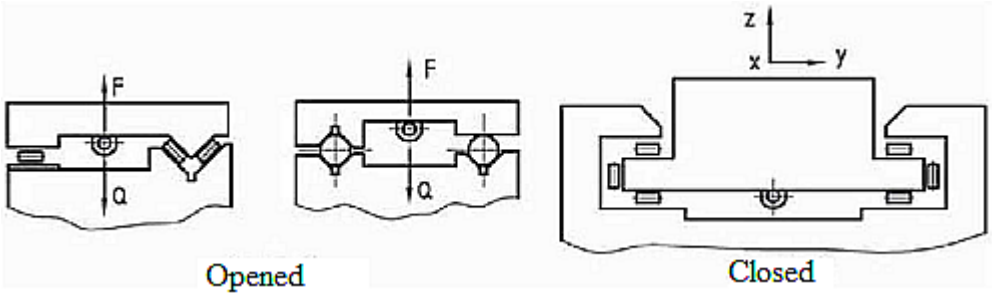

Fig. 2.6: Opened and closed guideways [1]

In the case of the guideway with unlimited length of stroke, the moving part can move along the entire length of the stationary part and distribute the nominal load during the movement. The basic element that allows this is a rolling block. It is mounted by screws mostly to the moving part of the guideway as shown in Fig.2.7. A certain number of rolling elements led by a cage circulates in a track that is created in the rolling block.

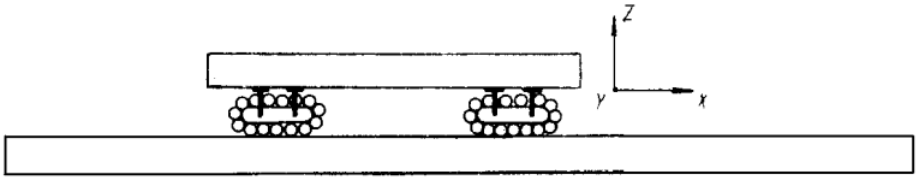

Fig. 2.7: Principle of a rolling guideway with unlimited length of stroke [1]

Rolling guideways with profiled tracks are nowadays most widely used in CNC machine tool design. Their mass use started with serial production of machine tools when the requirement on reliability of guideways increased. The first guideway of this type was developed in Germany in 1944 and it was a ball housing moving on a cylindrical rod. The principle of this guideway is based on circulating of the rolling elements along the profile of the rail. Rolling elements circulate inside the carriage and they are led by a cage. Typical composition of guideway with a profiled track is shown in Fig. 2.8.

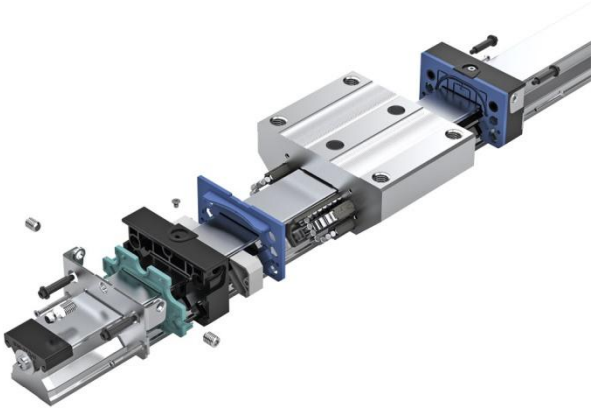

Fig. 2.8: Rolling guideway with profiled track – manufacturer SCHNEEBERGER [4]

It is apparent that linear guideways have a big effect on machine tool precision. The importance of dealing with thermo-mechanical behavior of linear guideways shows for example the 3rd generation of DMC V series made by one of the most significant manufacturers, DMG MORI. The machine has inner cooling circuits which keep the critical parts of the machine at stable temperature, including linear guideways [15]. The cooled guideway is pictured in Fig. 2.9.

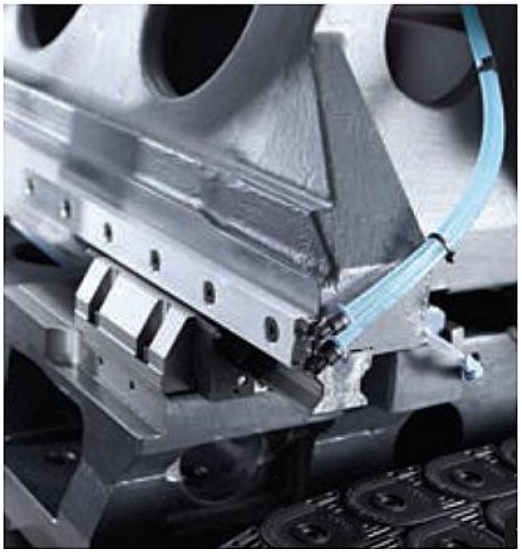

Fig. 2.9: Example of cooled linear guideways on DMG MORI DMC V series machine [15]

2.2 Disruptive thermal effects

Machine tools are affected by many heat sources during machining. These are dependent on load and time and they cause temperature changes of each structural group. That may cause undesirable deformations which have an unfavorable effect on accuracy [1].

Disruptive effects affecting thermal stability of machines can be divided according to Fig.2.10.

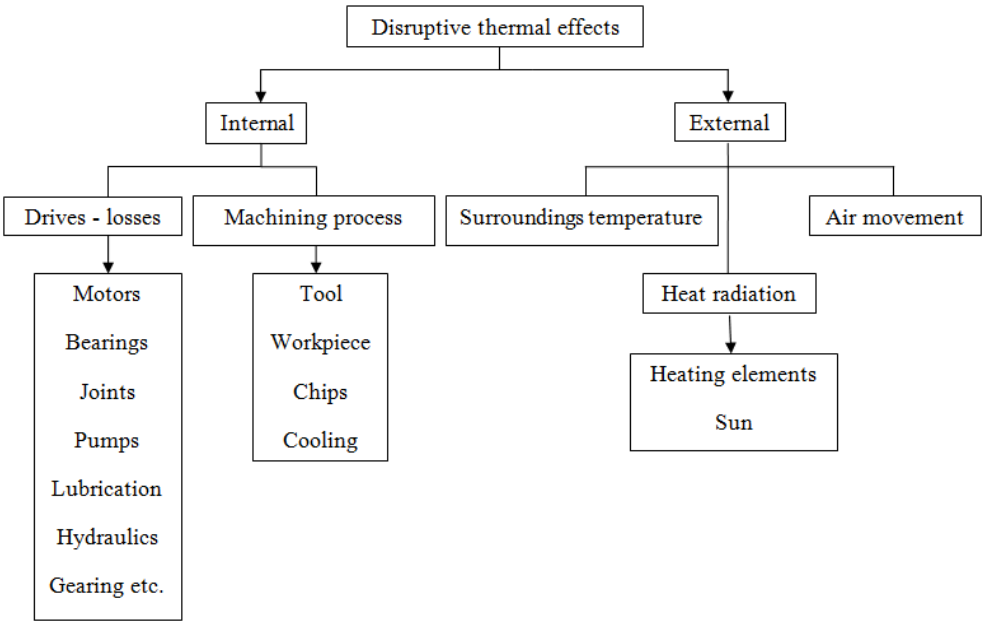

Fig. 2.10: Disruptive effects affecting machine tools [1]

External effects cause heat transfer on machine tool mainly by radiation and convection, contrariwise internal effects mainly by conduction [1].

2.3 Temperature measurement

Temperature is one the most important state variables affecting almost all states and processes in nature. When measuring temperature, it is not sufficient to use a precise thermometer and correct reading of data. It is also necessary to attach the thermometer properly so that it measures correctly [3].

Various physical principles can be used to measure temperature, for example thermal expansion of materials, dependency of electrical resistivity on temperature or formation of voltage. The basic temperature scale is the thermodynamic scale. Another

commonly used temperature scale is the Celsius scale [3]. All temperatures in this thesis are in Celsius scales.

2.3.1 Types of thermometers

Thermometers can be divided into contact and contact less. Contact thermometers are based on various physical principles and they are always in direct contact with the measured object. Contactless thermometers use thermal radiation that is emitted by the measured object [3].

2.3.1.1 Contact thermometers

To secure correct measurement with contact thermometers it is necessary to choose a suitable location of sensors in measured environment or object. The measured point should be chosen to allow the easiest possible mounting and dismounting of the sensor. To minimize the measurement errors it is important to secure the lowest possible heat losses from the sensor to the surroundings and also the highest possible heat transfer from the surroundings or object to the sensor. Contact thermometers can be divided according to the physical principles that are used to measure temperature [3].

a) Expansion thermometers

Expansion (or dilatation) thermometers use thermal dilatation of solids, liquids and gases. Based on their design they can be further divided into rod, bimetal, glass, liquid pressure or gas pressure. These types are here described only briefly; more information can be found in the literature [3].

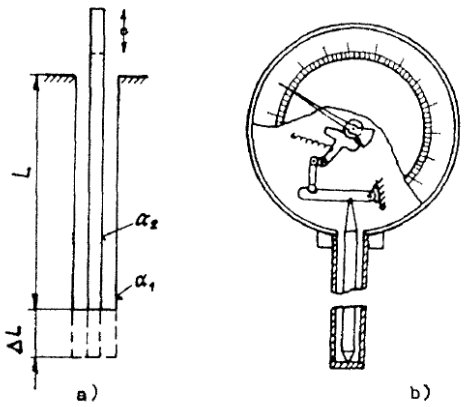

Fig. 2.11: Rod expansion thermometer: a) functional principal, b) technical execution

Rod expansion thermometers use different thermal dilatation of two separated parts – tube and inner rod. Heating of this system causes dilatation of the tube and the unattached end of the rod moves by ΔL according to the relationship:

$$\Delta L = L(\alpha_1 - \alpha_2)\Delta T \qquad (2.1)$$

Rod thermometers have a wide temperature range (up to 1,000°C) and they

are cheap. On the other hand, their disadvantages are lower accuracy, which is about 2%. Their use is mainly as sensors in two-position controllers, for example in thermostats [3].

Bimetal thermometers are made of metal plates of two materials which differ in thermal expansion. These plates are connected together along their entire length. During temperature change the plate deforms because of different thermal expansion. Like the previous type it is a simple structure whose main advantage is low price. It is used mainly for indicative measurements or as a sensor in two position controllers for temperature regulation [3].

Glass thermometers use thermal volume expansion of liquid in a glass capillary. The space above the liquid column in the capillary is evacuated or, for special thermometers, pressurized with inert gas to increase the range. Pentane mixture, mercury, toluene or ethyl alcohol is used as thermo measuring liquid [3].

Another type is liquid pressure thermometers. These consist of a bowl, connection capillary and measuring device – deformation barometer. The whole system is filled with liquid and temperature change causes pressure change, which is measured with deformation thermometer. Advantages of these thermometers are linear scale and relatively large measuring range. In recent years gas pressure thermometers have also been developed. Their design is similar to liquid pressure thermometers but they do not need any corrections. They are very precise with an error around 0.5% [3].

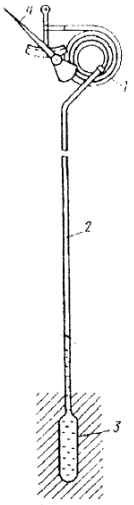

Fig. 2.12: Liquid pressure thermometer [3]

b) Resistance thermometers

Resistance thermometers use dependency of electrical resistance on temperature. This dependency is expressed with temperature coefficient of resistance α_R [K^{-1}]. Pure metals and semiconductors are primarily used to measure temperature. The most commonly used materials are summarized in Tab. 2.1.

Material	α_R [K^{-1}]	ρ_R [Ωm]	*Range [°C]*
Platinum	*0.00385 to 0.00391*	$9.81 \cdot 10^{-8}$	*-200 to 850*
Nickel	*0.00617 to 0.00675*	$12.13 \cdot 10^{-8}$	*-70 to +200*
Copper	*0.00426 to 0.00433*	$1.54 \cdot 10^{-8}$	*-50 to +150*
Thermistor	*-0.015 to -0.06*	---	*-80 to 200*
Electrolytes	*-0.015 to – 0.10*	---	*0 to 100*

Tab. 2.1: Materials used as measuring resistors [3]

The material that best meets the requirements on materials to be used as measuring resistors is platinum. Its thermal coefficient of resistance is relatively large and mainly time stable, which allows substitution of measuring resistors without additional verification. Platinum thermometers are among the most accurate and are even used as standards for verification of thermometers of all kinds. They are made in various designs such as ceramic, glass, pertinax and thin-film [3].

Ceramic measuring resistors have a platinum wire that has a diameter of about 0.05 mm. The wire is wound up in a helix and sealed into ceramic double-capillary. Basic thermometers are marked Ptk 100, thermometers with double winding DPtk 100 and special high-temperature measuring resistors DPvk 100. The value 100 in the marking indicates basic value of electric resistance at 0°C, 100Ω [3].

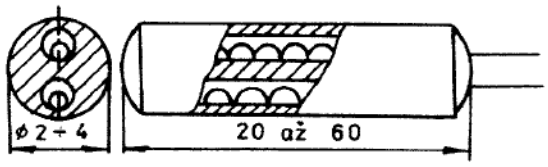

Fig. 2.13: Ceramic measuring resistor with platinum wire [3]

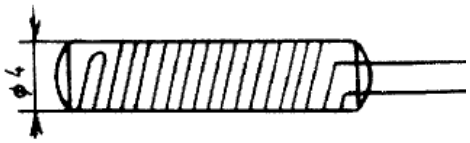

Fig. 2.14: Glass measuring resistor[3]

Glass measuring resistors have a platinum wire wound up bifilarly (Fig. 2.14) around a glass roller. The wire is moreover covered with a thin layer of glass. The disadvantage of this structure is strain phenomenon, which occurs due to different thermal expansion of glass and platinum [3].

Pertinax measuring resistors contains a platinum wire wound up bifilarly around a flat pertinax table. The system is externally insulated by a paper

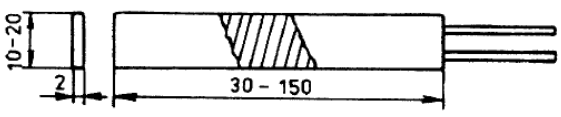

Fig. 2.15: Pertinax measuring resistor [3]

and lacquer. In comparison with previous thermometers, pertinax thermometers have a substantially lower range, up to about 150°C [3].

The last type of platinum thermometers is **thin-film thermometers.** It is this type that is used for temperature measurement in this thesis. They are made either by printing of platinum meander on a corundum pad or by application of a platinum paste which is then burned. They are very small, flat sensors used primarily for measuring surface temperatures. They are characterized by long-term stability [3].

Nickel is suitable material for measuring temperature mainly because of high thermal coefficient of resistance (almost 2x higher than platinum). However nickel thermometers have lower range compared to platinum thermometers, up to about 200°C. They are used for example in heat sensors in networks of central gas supply [3].

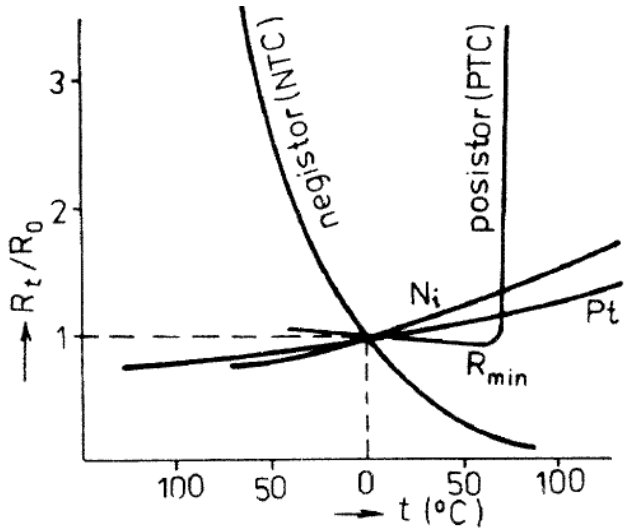

Fig. 2.16: Thermal dependency of chosen materials [3]

Thermistors are semiconductors whose sensitivity is about 10 times bigger than that of metals. A considerable disadvantage is, however, very nonlinear characteristic (see Fig.2.16). There are two types of thermistors – NTC and PTC. NTC have negative thermal coefficient of resistance, PTC positive. These days only NTC thermistors are used for measuring temperature. PTC thermistors are used as thermal fuses of winding of electric machines. Every thermistor must be calibrated individually because it is impossible to make two thermistors of similar characteristics. However, to make the substitution of thermistors possible, linearization can be done only in a narrow range of temperatures [3].

A diode can also be also used to measure temperature although it is not very common. When constant current flows through the forward direction of a diode, the voltage loss ΔU_D is dependent on temperature. Sensitivity of diodes depends on the type and size and the advantage is a linear characteristic as opposed to thermistors [3].

An interesting type are **crystal thermometers.** These include special faceted crystal that is connected to transistor resonance circuit. Changing of the crystal temperature causes a change of its resonance frequency and thereby a change of the frequency of oscillator whose oscillations interfere with oscillations of thermal independent reference oscillator. Thermal dependency of resonance frequency of the crystal is linear in the range from -80°C to +250°C with maximal deviation of 0.05%. That makes crystal thermometers the most accurate thermometers that are finding use in demanding applications such as calorimetry, cryogenics and during measuring of temperature fields [3].

c) Thermoelectric thermometers

Thermoelectric thermometers use a thermoelectric phenomenon. This phenomenon involves the creation of thermoelectric voltage on the interface of two different metal materials. The size of this voltage is directly proportional to the difference of temperatures of the contact of the two metals [3].

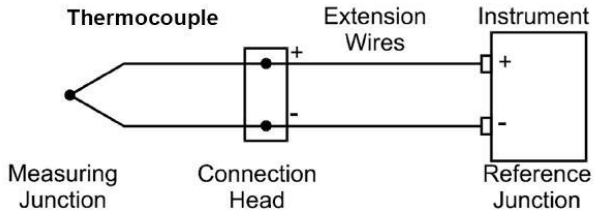

Fig. 2.17: Principal of thermocouple [5]

The couple of materials for manufacturing of a thermocouple should have the highest possible growth of thermoelectric voltage depending on temperature. It should be resistant to chemical and mechanical effects of the surroundings and it should give stable data during long-term use. The most widely used couples of materials in the area of middle temperatures in the industry are Fe-CuNi, Cu-CuNi, NiCr-Ni, NiCr-CuNi and NiCr-NiAl. For measuring of high temperatures thermocouples made of precious metals such as platinum, wolfram, rhodium and rhenium are used [3].

2.3.1.2 Contactless thermometers

Contactless thermometers use thermal radiation to measure temperature. They can be divided into directly measuring, so-called pyrometers and imaging (photographic and thermographic systems) [3].

2.4 Types of heat transfer

Heat transfer is thermal energy in transfer due to a spatial temperature difference. According to Fig.2.18, we refer to 3 modes of heat transfer. When a temperature gradient exists in stationary fluid or solid, we use the term conduction to refer to the heat transfer that occurs across the medium. On the other hand, the term convection refers to heat transfer that will occur between a surface and moving fluid when they are at different temperatures. Last mode of heat transfer is termed thermal radiation. All surfaces of finite temperatures emit energy in the form of electromagnetic waves [6].

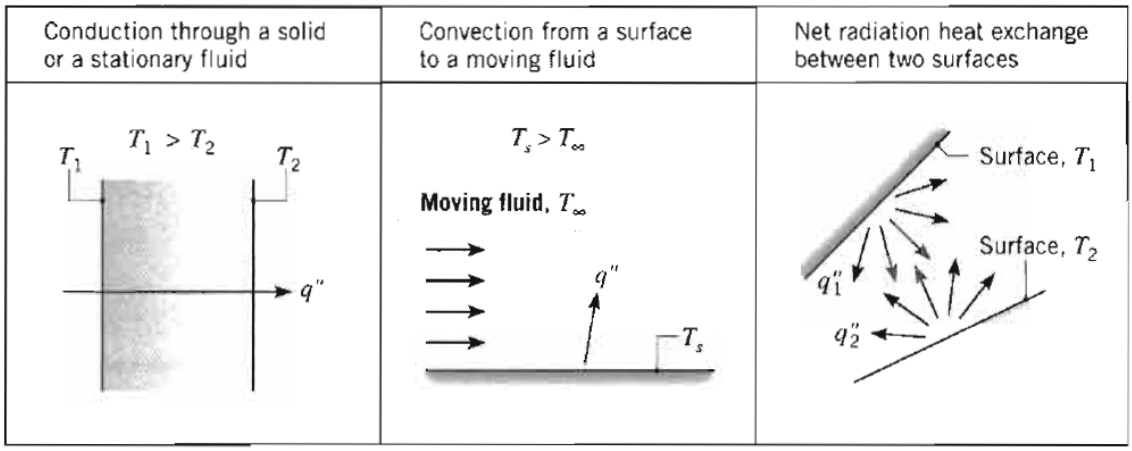

Fig. 2.18: Conduction, convection and radiation heat transfer modes [6]

2.4.1 Conduction

Conduction may be viewed as a transfer of energy from the more energetic to the less energetic particles of a substance due to iterations between the particles [6].

The amount of energy being transferred per time unit can be calculated using rate equations. For heat conduction, the rate equation is known as Fourier's law. For the one-dimensional plane wall shown in Figure 2.19, which has temperature distribution *T(x)*, the rate equation is expressed as [6]

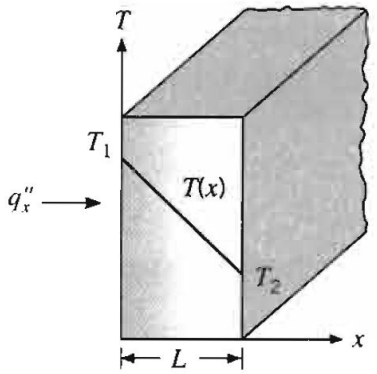

Fig. 2.19: One-dimensional heat transfer by conduction [6]

$$q_x'' = -k \cdot \frac{dT}{dx}, \tag{2.2}$$

where: $q_x^{"}$ … heat flux [W/m^2]

$\frac{dT}{dx}$ … temperature gradient [K/m]

k … thermal conductivity [W/(m·K)]

The heat flux $q_x^{"}$ is the heat transfer rate in the *x* direction per area unit. It is perpendicular to the direction of transfer and proportional to the temperature gradient $\frac{dT}{dx}$. Thermal conductivity *k* is a characteristic of the material. The minus sign is a consequence of the fact that heat is transferred in the direction of decreasing temperature. If the temperature distribution is linear, and the object is under steady-state conditions (see Figure 2.19), the temperature gradient may be expressed as [6]

$$\frac{dT}{dx} = \frac{T_2 - T_1}{L} \tag{2.3}$$

We can easily calculate the heat rate q_x [W] by conduction through the plane wall area *A* as a product of the heat flux $q_x^{"}$ and the area [6]

$$q_x = q_x^{"} \cdot A \tag{2.4}$$

2.4.2 Convection

Convection heat transfer occurs between a fluid in motion and a bounding surface when the two are at a different temperature. The thermal energy is transferred by bulk or macroscopic motion of the fluid. As it is shown in Figure 2.20, fluid flowing over heated surface results in a development of velocity and temperature distribution. Velocity varies from zero value at *y*=0 to a finite value u_x. This region of the fluid is known as a hydrodynamic or velocity boundary layer. As a result of the difference in temperatures of the flow and the surface, there is also a region of the fluid where temperature varies from T_s on the surface to T_∞ in the outer flow. This region of the fluid is called thermal boundary layer and it may be

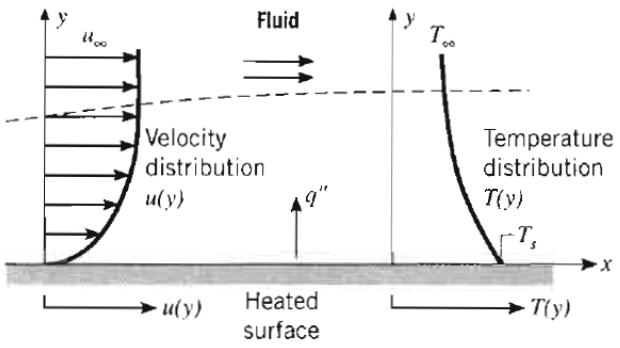

Fig. 2.20: Boundary layer development in convection heat transfer [6]

smaller, bigger or the same size as a velocity boundary layer. The convection heat transfer mode is sustained both by random molecular motion (diffusion) and by bulk fluid motion inside the boundary layer. Random molecular motion dominates near the surface where the speeds are low and on the surface where *y*=0 it is the only mechanism of heat transfer [6].

We can classify convection heat transfer according to the nature of the flow. If the flow is caused by external means (such as fan, pump or atmospheric wind), we speak about forced convection. On the other hand, we speak about free or natural convection when the flow is induced only by buoyancy forces, which occur due to density differences caused by temperature variations of the fluid [6].

The appropriate rate equation for the convection heat transfer is known as Newton's law of cooling and is expressed as [6]

$$q'' = h \cdot (T_s - T_\infty) \tag{2.5}$$

where: q'' …convective heat flux [W/m^2]

T_s …temperature of the surface [K]

T_∞…temperature of the fluid [K]

h …convection heat transfer coefficient [W/(m^2·K)]

Convection heat transfer coefficient *h* depends on conditions in boundary layer, which are influenced by surface geometry, the nature of the fluid motion and by the fluid thermodynamic and transport properties. Typical values of convection heat transfer coefficient are stated in Table 2.3.

Process	***h [W/(m^2·K)]***
Free convection:	
Gasses	*2-25*
Liquids	*50-1,000*
Forced convection:	
Gasses	*25-250*
Liquids	*100-20,000*

Convection with phase change:	
Boiling or condensation	*2,500-100,000*

Tab. 2.2: Typical values of convection heat coefficient [6]

2.4.3 Radiation

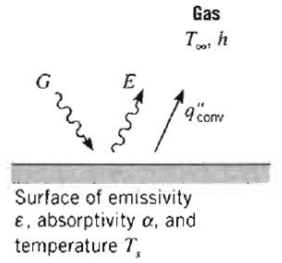

Fig. 2.21: Radiation exchange at a surface

Thermal radiation occurs when a substance is at nonzero temperature. It is a phenomenon when energy is emitted in the form of electromagnetic waves (or alternatively photons). The emission can be attributed to changes in electron configurations of atoms or molecules. As opposed to the energy transfer by conduction and convection, radiation doesn't require the presence of material medium. It occurs most efficiently in a vacuum [6].

Radiation transfer processes for surface are shown in Figure 2.21. Radiation emitted from the surface comes from the thermal energy that is bounded by the surface inside the object. Term emissive power, signed E_p [W/m^2], is a rate at which energy is released per unit area. The Stefan-Boltzmann law sets an upper limit to the emissive power and it is expressed as [6]

$$E_b = \sigma_E \cdot T_s^4 \tag{2.6}$$

where: E_b …upper limit of the emissive power [W/m^2]

$\sigma_E = 5.67 \cdot 10^{-8}$W/(m^2·K^4) … Stefan-Boltzmann constant [W/(m^2·K^4)]

T_s … absolute temperature [K]

Such a surface is called ideal radiator or blackbody. The heat flux emitted by a real surface is always smaller and it is given by [6]

$$E_p = \varepsilon \cdot \sigma \cdot T_s^4 \tag{2.6}$$

where ε is termed emissivity and it is a material property of the surface.

2.5 Thermal resistance

There exists an analogy between the diffusion of heat and electrical charge. Just as an electrical resistance is associated with the conduction of electricity, a thermal resistance may be associated with the conduction of heat. Defining resistance as the ratio of a driving potential to the corresponding transfer rate, the thermal resistance for conduction is [6]

$$R_T = \frac{T_1 - T_2}{q} \left[\frac{K}{W}\right] \tag{2.7}$$

A commonly used term especially when talking about heat transfer in composite walls is contact resistance. Contact resistance causes temperature drops on the interface of materials. The effect is shown in Fig. 2.22, and for an area unit of the interface it is defined as [6]

$$R_T^{"} = \frac{T_1 - T_2}{q^{"}} \left[\frac{Km^2}{W}\right] \tag{2.8}$$

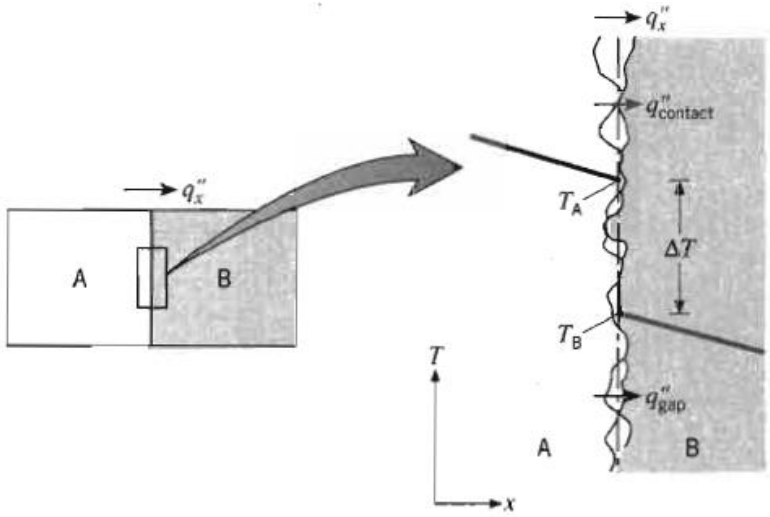

Fig. 2.22: Temperature drop due to thermal contact resistance [6]

Temperature drop is caused mainly by non ideal contact of the two mating materials. Due to a surface roughness and flatness deviation, only a part of the entire contact area is in real "metal to metal" contact, the rest is air gap. Interface materials that fill these air gaps between contacting materials can be used to increase or decrease the thermal contact resistance.

2.5.1 Parameters influencing thermal contact resistance

Thermal contact resistance is influenced by several factors. Some of them include properties of the two contacting materials and some are variable external parameters. The following parameters have an influence on thermal contact resistance [7].

a) Geometrical parameters – parameters such as **surface roughness (R_a)**, **flatness deviation (FD)** and **asperity slope (m or m')** influence the size of air gap in the contact area and thus the thermal contact resistance.

b) Pressure (P) – higher pressure on the contacting materials decreases the air gap and increases the contact area of the solids and therefore it is considered as a strong influential parameter.

c) Thermal conductivity of the contacting materials (k) – thermal conductivity of the contacting materials and interface material influence thermal contact resistance.

d) Surface hardness (H_c) or yield strength (S_Y) of the contacting materials – these parameters have an influence on plastic deformation of the contact area and thus also on the thermal contact resistance.

e) Young's modulus of elasticity of contacting materials (E) – this parameter describes elastic deformation of materials.

f) Linear coefficient of thermal expansion (α) – linear coefficient of thermal expansion can influence the behavior of the interface when temperature changes occur.

g) Average temperature of the interface (T_m) – average temperature influences physical properties of materials.

h) Gap thickness (δ) – gap thickness is an average value of distance between the two contacting materials.

2.6 Models for thermal contact conductance

Heat transfer through interfaces formed by the mechanical contact of two nonconforming rough solids occurs in a wide range of applications. Analytical, experimental and numerical models have been developed since the 1930s to cover the need of quantifying thermal contact conductance [8]. In this chapter, some of these models are described.

Firstly, some basic parameters and correlations later commonly used in thermal conductivity models will be described. The effective thermal conductivity k_s can be calculated as

$$k_s = \frac{2k_1k_2}{k_1+k_2} \tag{2.9}$$

where indices 1 and 2 represent the two materials of the joint.

Roughness of a surface is commonly described by arithmetic average of roughness R_a which is given by

$$R_a = \frac{1}{L}\int_0^L |y(x)|dx \tag{2.10}$$

and also by RMS roughness σ which is defined as

$$\sigma = \sqrt{\frac{1}{L}\int_0^L y^2(x)dx} \tag{2.11}$$

where y is the distance of the surface from the mean plane and L is the length of the trace. Similarly, RMS asperity slope m' can be obtained from absolute asperity slope m and if we assume Gaussian distribution of asperities we can calculate it as

$$m' = \sqrt{\frac{\pi}{2}}m \approx 1.25m \tag{2.12}$$

similarly for the roughness with assumption of Gaussian distribution of asperities

$$\sigma = \sqrt{\frac{\pi}{2}}Ra \approx 1.25R_a \tag{2.13}$$

If two materials with different roughness and asperity slopes are in contact, effective values of these parameters are commonly stated in mathematical models that

describe thermal heat conductance. Effective values of RMS roughness and effective absolute asperity slope are calculated as

$$\sigma_s = (\sigma_1^2 + \sigma_2^2)^{1/2} \tag{2.14}$$

$$m_s = (m_1^2 + m_2^2)^{1/2} \tag{2.15}$$

For better illustration absolute surface slope *m* and RMS surface roughness are shown in Fig. 2.23.

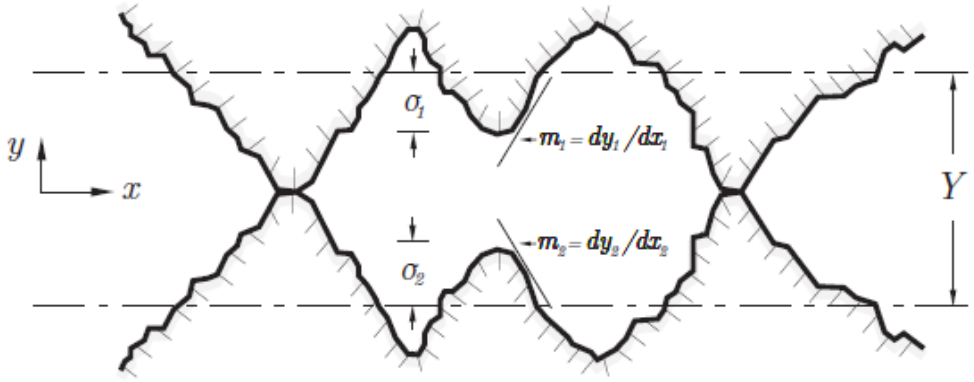

Fig. 2.23: Two surfaces in contact, showing surface asperities parameters – absolute surface slope m and RMS surface roughness σ [7]

2.6.1 Elastic models

Elastic models assume elastic deformation of the contact area. This generally leads to a model which depends on Young's modulus of elasticity *E*. The following text shows theoretical and empirical models for thermal contact conductance.

a) Model by Fletcher and Gyorog

In 1970 Fletcher and Gyorog suggested a model for quantifying thermal contact conductance. This model relates material properties, surface finish, contact pressure and mean joint temperature to resulting contact conductance and it was determined empirically. The model was also compared with empirical data from other studies and the average overall error was concluded less than 24% [7]. The thermal contact conductance by Fletcher and Gyorog is given by

$$h_c = \frac{k_s}{\delta_0}\left[5.22 \cdot 10^{-6}\frac{\delta_0}{r} + 0.036 \cdot \frac{P}{E}\alpha T_m\right]^{0.56} exp\left[170\frac{P\alpha T_m r}{E\delta_0}\right] \tag{2.9}$$

where *r* is the radius of cylindrical joint interface and δ_0 is gap thickness parameter, which is given by

$$\delta_0 = 5.194 \cdot 10^{-7} + 8.060 \cdot 10^{-2} s - 6.220 \cdot 10^{-2} s^2 + 2.108 \cdot 10^{-6} s^3 \quad (2.10)$$

where *s* is parameter of surface given by

$$s = (FD + 2R_a)_{rough} - \frac{1}{2}(FD + 2R_a)_{smooth} \quad (2.11)$$

Symbols α, E, T_m, P, k, FD and R_a are parameters influencing thermal contact conductance as was described in 2.5.1. Indices *rough* and *smooth* in equation (2.11) stand for rougher and smoother surface of the contact joint materials, if they have different roughness [7].

b) Model by Mikic

The model derived analytically by Mikic in 1974 is assuming elastic deformation. The thermal contact conductance is given by

$$h_c = 1.55 \cdot \frac{k_s m_s}{\sigma_s} \left(\frac{P\sqrt{2}}{E' m_s} \right)^{0.94} \quad (2.12)$$

where *E'* can be obtained from Young´s modulus of elasticity *E* and Poisson´s ratio *v*. It is given by

$$E' = \frac{E_1 E_2}{E_2(1-\nu_1^2) + E_1(1-\nu_2^2)} \quad (2.13)$$

At least three similar formulas to equation (2.12) with different numerical constants were derived (Greenwood and Williamson in 1966, Onions and Archard in 1973, Bush, Gibson and Thomas in 1975).

Mikic then neglected the influence of m_s from his model and used m_s =0,1 (average for blasted surfaces) which led to a simplification of equation (2.12). The thermal contact conductance is then given by

$$h_c = 1.9 \cdot \frac{k_s}{\sigma_s} \left(\frac{P}{E'} \right)^{0.94} \quad (2.14)$$

Equation (2.19) is practical because only pressure *P* and surface roughness σ_s needs to be measured to calculate the thermal contact conductance.

2.6.2 Plastic models

Assuming plastic deformation generally leads to a model that depends on the surface hardness $H_{C.}$

a) Model by Cooper, Mikic and Yovanovich

In 1969, Cooper, Mikic and Yovanovich deduce a relationship between applied pressure, material properties and thermal contact conductance. The established relationship was then fitted to experimental data and the proposed model for thermal contact conductance is given by:

$$h_c = 1.45 \cdot \frac{k_s m_s}{\sigma_s} \left(\frac{P}{H_C}\right)^{0.985} \tag{2.15}$$

The model (2.15) correlated well with the experimental data, but its absolute error is between 50-100% [7].

More models similar to (2.15) were established. They differ in numerical constants and are more accurate for specific materials and conditions.

2.7 Heat transfer across machine parts

In the field of production machines and especially machine tools, it is important to understand the principles of heat transfer across single parts to avoid or be able to compensate thermal deformations.

2.7.1 Bolted joint

In [9], Mantelli analytically describes heat transfer across typical bolted joint in satellites. It consists of upper and lower plate, bolt, nut and washers that are placed under the bolt head, between plates and under the nut. The assembly is shown in Fig. 2.24.

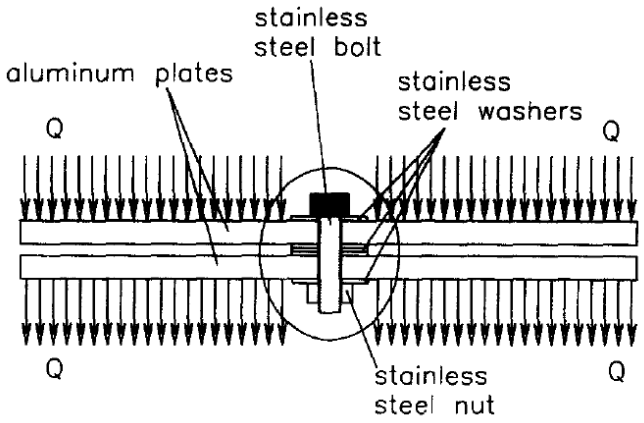

Fig. 2.24: Typical satellite bolted joint

Heat is supplied to the upper plate and dissipated from the lower plate. To model the overall thermal resistance of the bolted joint, an analogy to electrical circuit can be used. The whole thermal resistance network is illustrated in Fig. 2.25, where R_c indicates contact resistances, R_m material resistances and R_{ct} constriction resistances. Subscript w_0 refers to the washer under the bolt head, w_1 to w_n to the washers between the plates and w_{n+1} to the washer between the lower plate and the nut. In surroundings of the bolt, heat follows one of two paths: either through the washers between the plates or through the bolt. These two paths are thermally connected in parallel. The third parallel path, the radiation resistance path, is shown by dashed lines because in most applications its value is much larger in comparison with other parallel resistances and therefore it can be neglected.

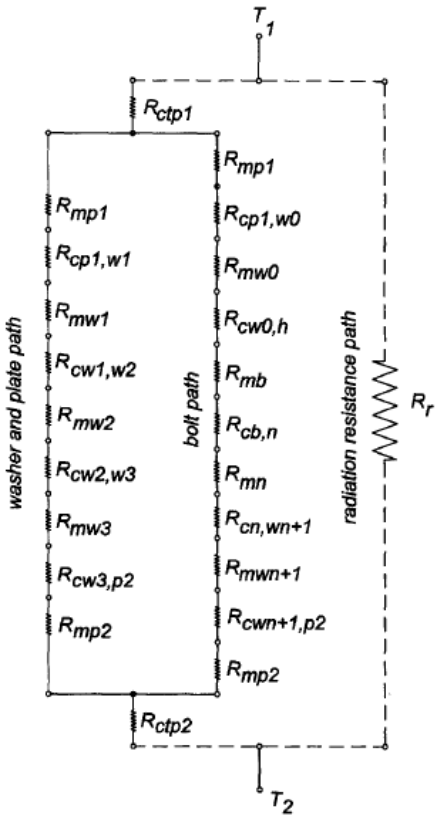

Fig. 2.25: Thermal resistance network for the bolted joint [9]

2.8 Experiments for thermal resistance investigation

This chapter describes experiments for thermal resistance investigation. Figure 2.26 shows a generalized schematic setup of the experiment. Main parts of the setup are the measured piece, a heat source and two thermometers – one on the top of the measured piece and one at the bottom. The whole assembly is thermally insulated from the surroundings.

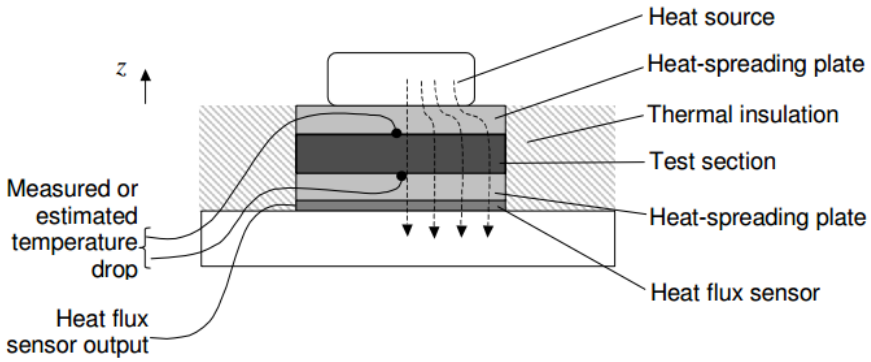

Fig. 2.26: Schematic representation of a generalized thermal conductivity setup[14]

The two measured temperatures allow us to determine the temperature drop T_1-T_2, which is the first crucial parameter for determination of thermal resistance, according to equation (2.7). The second crucial parameter is heat rate produced by heat source. If the heat source is an electrical resistor, the heat rate is given by

$$q = U \cdot I = \frac{U^2}{R}[W] \tag{2.16}$$

Following chapters 2.8.1, 2.8.2 and 2.8.3 describe specific applications of experiments for thermal resistance investigation.

2.8.1 Bolted joint experiment

In [7], thermal contact conductance of a bolted joint is experimentally investigated. The experiment consists of a rectangular top and bottom plate. The bottom plate has countersunk holes for bolts and threaded holes were drilled into the upper plate. Several top and bottom plates were made with different surface roughness and from different materials. The layout of the experiment is illustrated in Fig. 2.27.

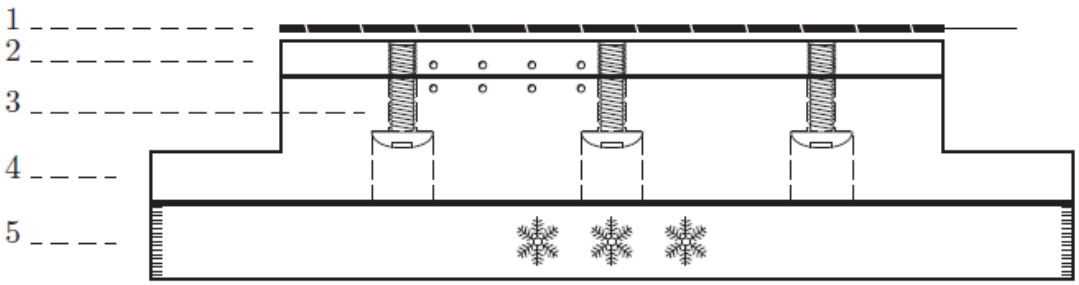

Fig. 2.27: Layout of bolted joint experiment. 1-heater, 2-top plate, 3-bolts, 4-bottom plate, 5-cooled base plate [7]

Four holes were drilled horizontally as close as possible to the interface surface in both plates. These holes enabled placement of the thermocouples in the center of the joint. In total, eight thermocouples were mounted in each set of bolted joints, enabling measurement of the interface temperature drop ΔT at four separate locations. The experiment was placed into a vacuum chamber to avoid thermal losses into surroundings.

2.8.2 Cylinder joint experiment

In [7], another layout of experiment for thermal contact conductance investigation can be found. It consists of two cylinders that are pressed together and it was conducted to investigate the relation between thermal contact conductance and pressure.

The layout is illustrated in *Fig. 2.28*. Different levels of load were applied in the axial direction of the columns using a screw rig. A piezoelectric force sensor is placed in the assembly to measure the applied force. There are also insulating cylinders placed at the top and bottom that prevent heat conduction from the interface.

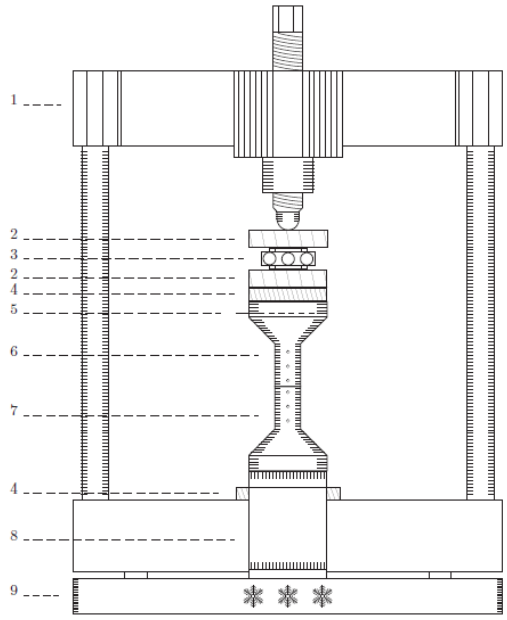

Fig. 2.28: Layout of cylinder joint experiment. 1-Rig, 2-Spacer, 3-Force sensor, 4-Insulation, 5-Heater, 6-Top cylinder, 7-Bottom cylinder, 8-Aluminum plate, 9-Cooled base [7]

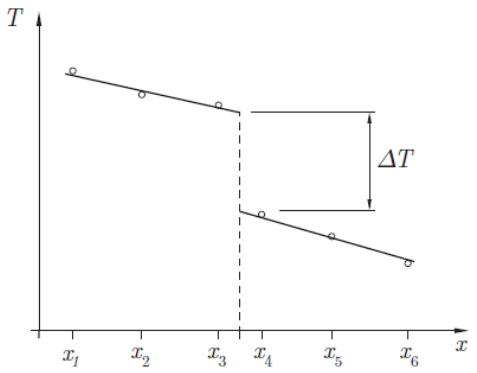

Fig. 2.29: Illustration of temperature profiles for the estimation of interface temperature gap [7]

Three thermocouples were placed in holes that were drilled perpendicular to the centerline in both cylinders. This enabled temperature measurement at different distances from the interface and therefore the calculation of temperature gradient in both cylinders. The temperature gradient then allows us to evaluate the temperature gap at the interface, as is illustrated in *Fig. 2.29*.

2.8.3 Measurement of heat transfer through linear guideways

In a master´s thesis [10], an experimental investigation of thermal resistance of linear guideways is executed. The measurement was done with one linear guide. Different values of external load were applied using a hydraulic valve to investigate the relationship between load and thermal resistance. The layout of experiment is pictured in Fig. 2.30.

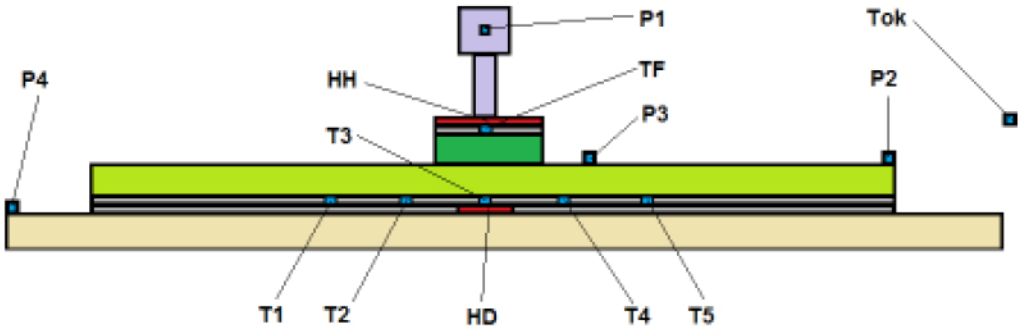

Fig. 2.30: An experiment to investigate thermal resistance of linear guideways. T1,T2,T3,T4,T5 – thermocouples placed inside material, P,P2,P3,P4 – thermocouples on the surface, Tok – ambient temperature, HD – heater at the bottom, HH – heater at the top.

Figure 2.31 shows results of measurement with different levels of external load. It is apparent that with higher load, the difference in temperatures at the top (TF) and at the bottom (T3) is lower. This means that thermal resistance gets lower with growing load.

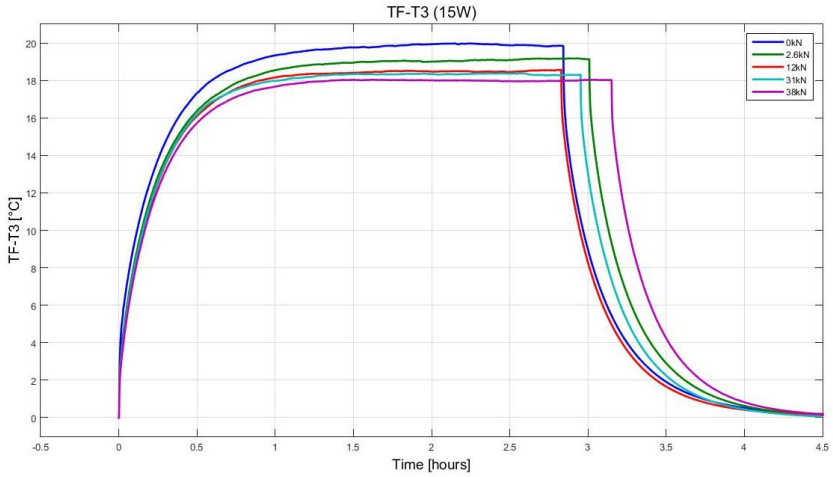

Fig. 2.31: Dependency of temperature difference (TF-T3) on external preload. Heat rate during measurement was 15W [10].

Apart from the mentioned case, no other literature dealing with investigation of thermal resistance of linear guideways was found in scholarly literature or in documents provided by manufacturers.

Other experiments done on linear guideways can be found in literature. Their aim was not to investigate the thermal resistance, but they also deal with thermo-mechanical properties of guideways. E.g. in [16], a few experiments investigating thermo-mechanical properties of linear guideways can be found.

Firstly, the influence of velocity and load on friction force and thereby the heat output were investigated on a test rig designed for that purpose. The setup of the test rig is schematically shown in Fig. 2.32. Two equal guide systems are mounted opposite each other above and beneath the traverse of the test rig structure. Load is applied using a load unit with a strain sensor, which measures the load directly. The rails are fixed to the traverse and the shoes are driven by a linear motor which is coupled with the movable unit via a force sensor to measure the friction force of the guide system. By separating the motor from the movable unit, the heat generation by the motor has no influence and can be neglected. The only heat source in the considered system is friction of the guide systems. Temperatures are measured with several integrated thermocouples and resistance temperature detectors Pt100 [16].

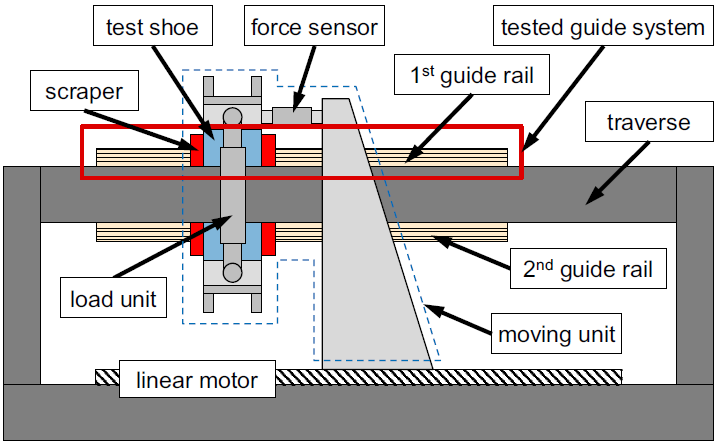

Fig. 2.32: Schematic setup of the test rig [16]

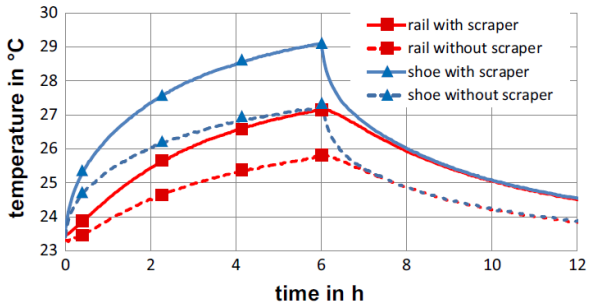

Fig. 2.33: Temperature distribution with and without scraper, load 5,000N, velocity 40m/min [16]

To determine what amount of the friction loss is generated by the scraper of the shoe, experiments with and without the scraper were conducted. Figure 2.33 shows the

temperature in the guide rail and the shoe with only one measurement point for each case. In both experiments the other parameters (velocity and load) are kept constant. During the first 6 hours, the test rig operates and heats up and then it is stopped and cools down. Two phenomena can be identified: First, in contrast to the shoe, the guide rail with the scraper reveals an additional increase in temperature of 1°C. Second, without a scraper, temperatures are almost identical within the shoe and the rail but lower than those measured in the previous experiment. This leads to the assumption that most of the heat generated by the scraper is transferred to the rail [16].

The second modified parameter is velocity. The resulting temperatures are shown in Fig.2.34. As expected the highest temperatures occur in the experiment with the highest velocity of 40m/min. The highest difference between shoe and rail temperature constitutes about 2°C [16].

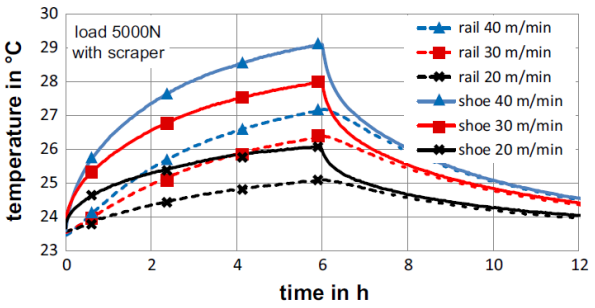

Fig. 2.34: Temperature distribution depending on the velocity, load 5,000N, with scraper [16]

The experiment was then repeated with different values of load, velocities and with or without scraper and friction power was calculated. The results are shown in Table 2.3. It is shown that, as expected, the friction increases with velocity.

Velocity in m/min	Load in N	Scraper	Friction power in W
20	1,100	Yes	18.01
20	3,250	Yes	18.86
20	5,000	Yes	22.57
30	1,100	Yes	37.19
30	3,250	Yes	34.60
30	5,000	Yes	42.82
30	5,000	No	33.69
40	1,100	Yes	50.66
40	3,250	Yes	43.83
40	5,000	Yes	56.92
40	5,000	No	46.27

Tab. 2.3: Friction power for different loads, velocities and usage of scrapers [16]

3 Experiment for determination of thermal resistances of linear guideways

This chapter describes an experiment that was proposed for determination of thermal resistances of linear guideways.

3.1 Experimental setup

The main requirement on the experiment was to thermally insulate the linear guideways from the surroundings. An ideal way to achieve this is to place the whole assembly in a vacuum chamber, as it was done in the experiment described in chapter 2.8.1. This will cause that the heat losses will be only by radiation. In the experiment described in chapter 2.8.3., the linear guide is screwed to a base plate and the whole assembly is placed in a laboratory and surrounded by air. The disadvantage of this layout is that the movement of air can highly affect results as some thermometers are placed on the surface. Also, thermal losses to the base plate are very high and unpredictable.

As there was no access to the vacuum chamber in the laboratory, the insulation was made of polystyrene. The advantage of polystyrene insulation is that the effect of ambient temperature changes and heat losses to the surroundings will be minimal. A complete scheme of the assembly is pictured in Fig. 3.1, and a photograph taken during installation can be seen in Fig. 3.2.

It consists of the measured linear guide, a heating foil placed on the top of the carriage and 9 resistance thermometers. 4 resistance thermometers were placed on the vertical axis of the assembly and 4 on the left side from the vertical axis, since the symmetry was assumed. The last thermometer measured ambient temperature. A spacer with a groove was placed on the top of the carriage and under the heater to enable the placement of thermometer *T1*. The whole assembly is covered in polystyrene insulation. The polystyrene insulation was made on a wire cutter from Synthos Prime XPS polystyrene boards with a coefficient of thermal conductivity *k=0.036 W/(mK)*, density ρ=35 kg/m^3 and specific heat *C*=2060J/(kgK), as stated by the manufacturer.

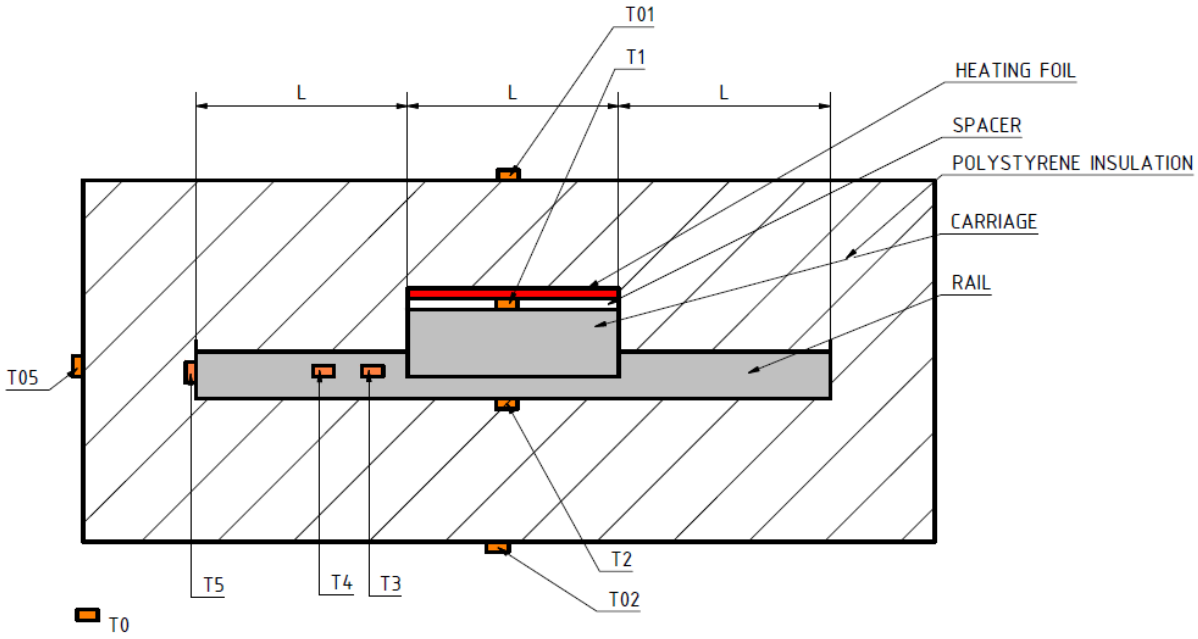

Fig. 3.1: Experimental setup proposed for determination of thermal resistances of linear guides. T1 – temperature on the top of the carriage; T2 – temperature on the bottom of the rail; T3, T4 and T5 – temperatures on the rail;, T01, T02 and T05 – temperatures on the surface of polystyrene; T0 – ambient temperature

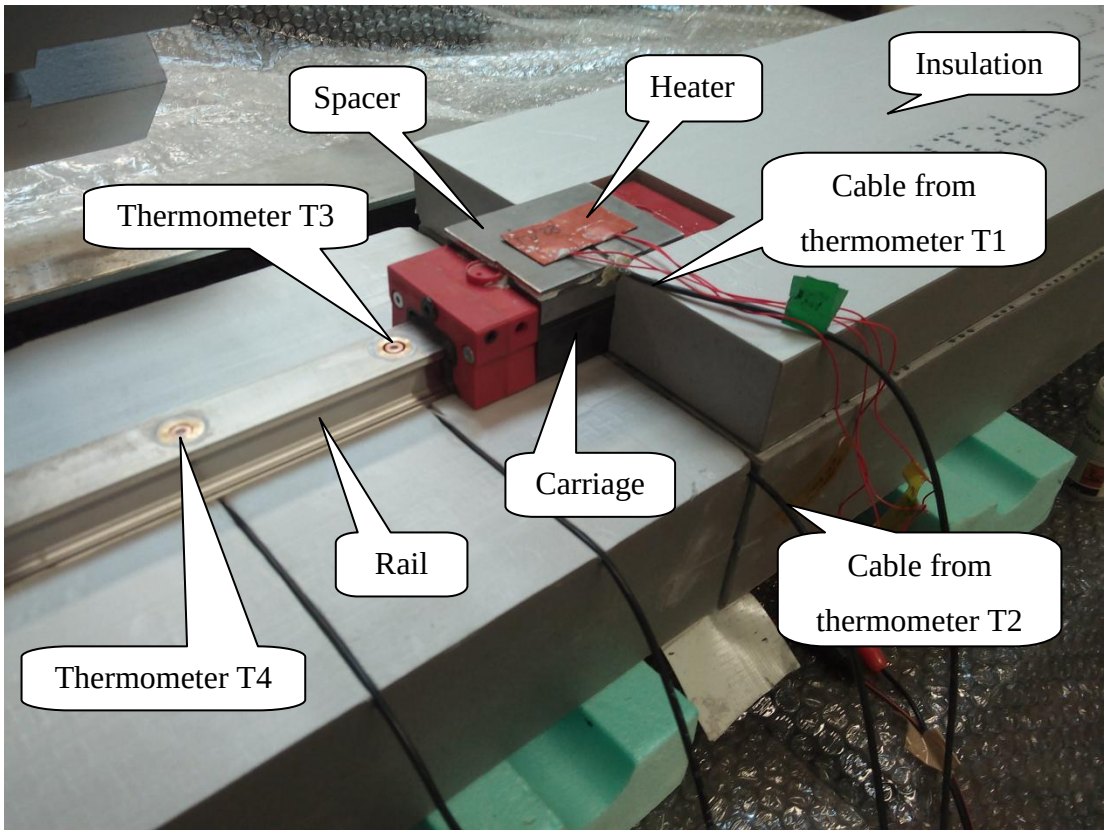

Fig. 3.2: Photograph of the assembly taken during experiment installation

Thermometers *T1*, *T2* and *T5* were attached to the linear guide with silicone. Special cases from brass were made for placement of thermometers *T3* and *T4* in holes for screws in the rail. Other holes for screws in the rail were filled with steel plugs made for that purpose in order to make the experiment conditions similar to real state on the machine. A thin film of thermally conductive paste was used between thermometers and measured contacts, between the heater and spacer and also between the spacer and carriage.

Two same heaters from manufacturer MINCO were used for heating. Each heater has resistance R=78.4Ω and dimensions of (25.4 x 25.4) mm. Catalogue number of this type is HR5163R78.4L12.

3.2 Specification of measured linear guideways

The aim of this work is to measure linear guideways differing in size, preload and type of rolling elements and evaluate the effect of these parameters on thermal resistance of linear guideways.

Order number from the catalog	Part description	Size	Preload class	Rolling elements
MR S 35 N-G2-KC-R1-408-24-24-CN	Rail for MR carriage	35	-	-
MR W 35 B-G2-V1-R1-CN-S10-LN	MR carriage, wide type	35	V1	rollers
MR W 35 B-G2-V3-R1-CN-S10-LN	MR carriage, wide type	35	V3	rollers
BM S 35-N-G2-KC-R1-411,5-45,75-CN	Rail for BM carriage	35	-	-
BM W 35 B-G2-V1-R1CN-S00-LN	BM carriage, wide type	35	V1	balls
BM W 35 B-G2-V3-R1CN-S00-LN	BM carriage, wide type	35	V3	balls
MR S 45 N-G2-KC-R1-517,5-22,5-22,5-CN	Rail for MR carriage	45	-	-
MR W 45 B-G2-V3-R1-CN-S99-LN	MR carriage, wide type	45	V3	rollers
MR S 55 N-G2-KC-R1-616,5-38,25-38,25-CN	Rail for MR carriage	55	-	-
MR W 55 B-G2-V3-R1-CN-S99-LN	MR carriage, wide	55	V3	rollers
MR S 65 N-G2-KC-R1-616,5-38,25-38,25-CN	Rail for MR carriage	65	-	-
MR W 65 B-G2-V3-R1-CN-S99-LN	MR carriage, wide type	65	V3	rollers

Tab. 3.1: Specifications of measured linear guideways produced by SCHNEEBERGER

For this purpose, one of the biggest manufacturers of linear guideways, SCHNEEBERGER, supplied different types of their linear guideways. Detailed specification of the supplied linear guideways can be seen in Table 3.1.

The preload classes are dependent on the dynamic loading capacity, signed C_{100} [4]. Preload of class V1 is given by:

$$F_{V1} = 0.03 \cdot C_{100} \tag{3.1}$$

and preload of class V3 is given by:

$$F_{V3} = 0.13 \cdot C_{100} \tag{3.2}$$

Preload forces were calculated for measured guideways according to equations (3.1) and (3.2) and they are stated in Table 3.2.

	MRW35	**MRW45**	**MRW55**	**MRW65**	**BMW35**
C_{100} [N]	71,500	127,800	180,500	295,000	46,700
F_{V1} [N]	2,145	-	-	-	1,401
F_{V3} [N]	9,295	16,614	23,465	38,350	6,071

Tab. 3.2: Preload forces for measured guideways

The carriages of MRW and BMW guideways are both made of carbon steel 100CrMo7-3. Rail of BM type of guideway is made of C53G steel and rail of MR type is made of 58CrMoV4 carbon steel. Thermal conductivity *k*, density ρ and specific heat *C* of these materials are stated in Table 3.3.

Material	*k [W/m·K]*	*ρ[kg/m^3]*	*C[J/kg·K]*
100CrMo7-3	39	7840	477
58CrMoV4	40	7800	470
C53G	42.7	7840	460

Tab. 3.3: Properties of guideways materials

3.3 Uncertainty of measurement

Every measurement is influenced by various negative effects that occur during the measuring process. This results in deviation between the real and measured value of monitored physical quantity. The result of measurement is always stated in a certain interval in which the real value is situated with high probability [11].

We divide uncertainties into two main categories:

a) Type A

This type is usually used during repeated measurements. It uses statistics to estimate the value of uncertainty. Since there is no repeating during this measurement, uncertainty of type A is $u_A=0$.

b) Type B

Uncertainty of type B is given by imperfection of measuring devices, methods, conditions during measurements and by the human factor.

Uncertainty of type B consists of two parts. The first is deviation of thermal resistor RTD PT 100A and the second is the deviation of the data logger NI cDAQ 9188. According to [12], the deviation of RTD PT100A for measured temperature 50°C is ±0.25°C. Uncertainty of type B for RTD PT100A is then given by:

$$u_{B(PT100)} = \frac{0.25}{2} = 0.125°C \tag{3.3}$$

Uncertainty of data logger NI cDAQ 9188 consists of two parts. The first is error of the device, which is ±0.3°C in a measuring range of 50°C according to calibration certificate. The first uncertainty of NI cDAQ 9188 is given by:

$$u_{B1(cDAQ)} = \frac{0.3}{2} = 0.15°C \tag{3.4}$$

The second uncertainty of NI cDAQ 9188 is the error of reading, which is the smallest possible value of measured temperature – 0.00001°C. Uncertainty for his error is given by:

$$u_{B2(cDAQ)} = \frac{0.00001}{\sqrt{3}} = 5.773 * 10^{-6}\ °C \tag{3.5}$$

Combined standard uncertainty of logger NI cDAQ 9188 is then given by:

$$u_{B(cDAQ)} = \sqrt{u_{B1(cDAQ)}{}^2 + u_{B2(cDAQ)}{}^2} = \sqrt{0.15^2 + (5.773 * 10^{-6})^2} = 0.15°C \quad (3.6)$$

And combined standard uncertainty of type B is given by:

$$u_B = \sqrt{u_{B(PT100)}{}^2 + u_{B(cDAQ)}{}^2} = \sqrt{0.125^2 + 0.15^2} = 0.195°C \quad (3.7)$$

Expanded uncertainty of measurement is given by:

$$U_M = c * u_B = 2 * 0.195 = 0.39°C \quad (3.8)$$

where *c* is called *coverage factor*. Using the coverage factor *c=2* gives us a level of confidence of approximately 95% for normal distribution [13].

4 Measurements results

This chapter presents the results of executed measurements and compares them with each other and with measurement done in [10]. All measurements had to be stopped when *T1* reached 50°C, because at higher temperatures the polystyrene insulation started to degrade. The measured results from thermometers placed inside the insulation are presented graphically in this chapter. Temperatures measured on the outside of insulation can be found in Appendix A.

4.1 Linear guideway SCHNEEBERGER BMC30 (balls rolling elements)

This type of linear guideway was measured in [10] and it is measured in this thesis mainly to compare the results, as the layouts of both experiments are different. The layout of experiment executed in [10] is described in chapter 2.8.3 and the layout of experiment executed in this thesis is described in 3.1.

Figure 4.1 shows results of measurement with heat rate set to 15W.

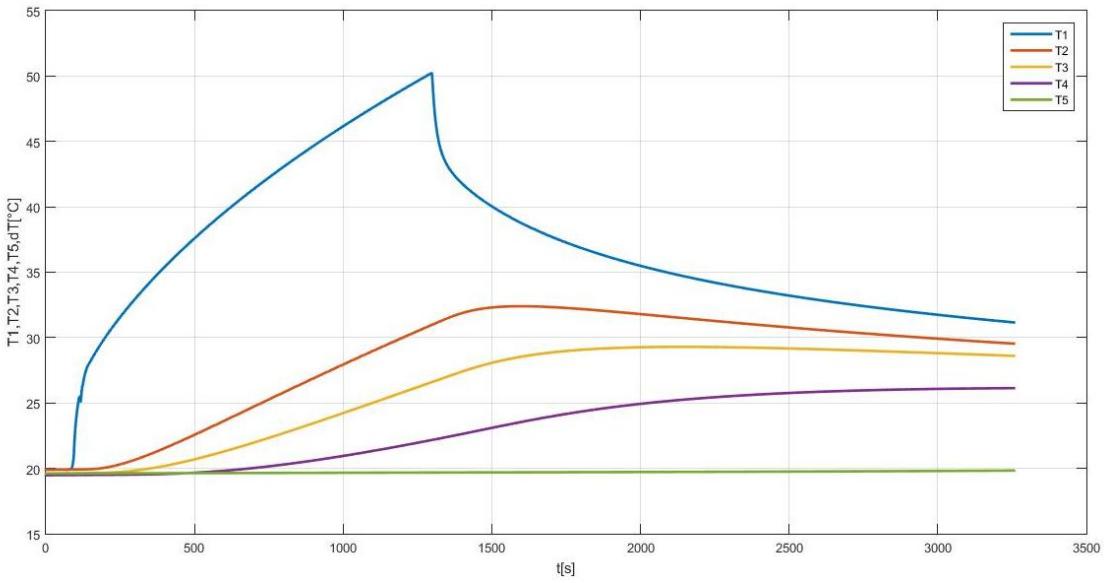

Fig. 4.1: Results of measurement of BMC30 guideway with heat rate 15W

For the evaluation of thermal resistance, the main parameter is temperature difference between the top and the bottom of the linear guideway *dT=T1-T2*. *Figure 4.2* compares the temperature differences between the top and the bottom of the guideway.

The blue curve is the temperature difference measured in the experiment with insulation and the orange curve is a result from [10]. It can be seen that *dT* is still slowly growing when the experiment had to be stopped. For this reason, *CurveFit tool* in *Matlab* was used to fit a mathematical function to the measured curve. This function helps us to estimate temperature difference *dT* in steady state. Best results were obtained with function given by:

$$dT = 21{,}46 - 4{,}732 \cdot e^{-\frac{t}{16{,}35}} - 10{,}28 \cdot e^{-\frac{t}{781{,}3}} - 5{,}206 \cdot e^{-\frac{t}{146{,}4}} \tag{4.1}$$

where *t* is time.

The quality of fit can be indicated by *R-square*, which is a number that indicates how well the data fit the mathematical model. In this case *R-square* is 0,9997; which is a sufficient value.

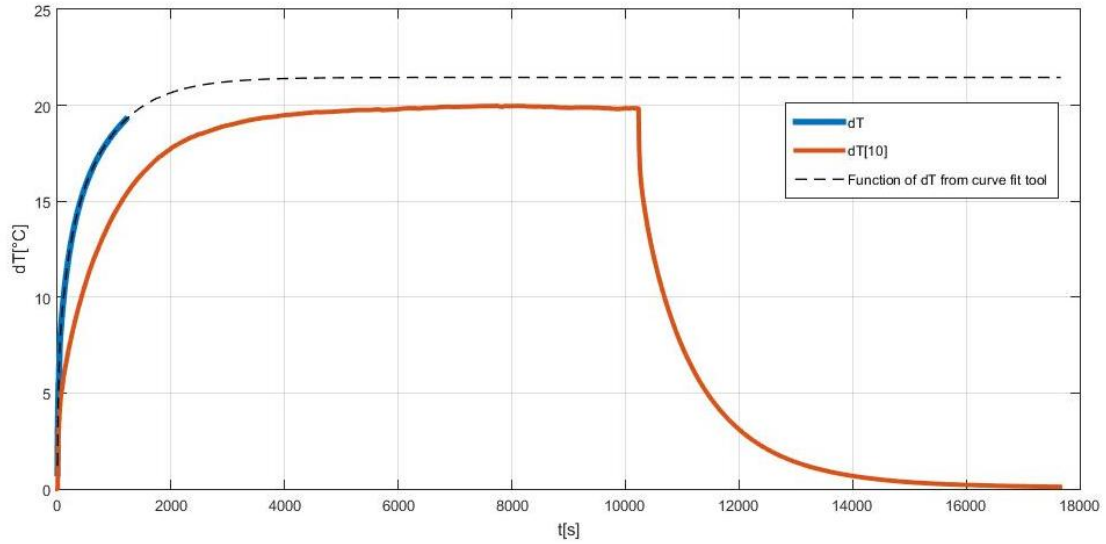

Fig. 4.2: Comparison of temperature differences dT

From Figure 4.2, it is apparent that in the experiment where the linear guide was insulated, the temperature difference *dT* grows quicker. It can also be seen that the temperature difference *dT* is not equal in both experiments: 21.5°C in the experiment with insulation and 19.9°C in the experiment where the guideway was placed on the base plate. The difference in *dT* between both measurements is

$$\Delta dT = dT_{insul} - dT_{mount} = 21.5\text{-}19.9 = 1.6\ °C \tag{4.2}$$

This means there will be differences in the values of temperature resistance evaluated from the measurement. Reason is that in the experiment where guideways is mounted to the base plate, there are bigger heat losses to the surroundings. Therefore result from the experiment with insulation should be more accurate.

4.2 Linear guideway SCHNEEBERGER MRW35 (rollers rolling elements)

Two types of this guideway differing in size of preload were measured. The lighter class signed V1 and heavier class signed V3. Comparing these two types should show dependency of thermal resistance on the size of preload in the case of roller linear guideways.

4.2.1 MRW35-V1

The measurement was done with heat rate set to 10W. Figure 4.3 shows the results of measured temperatures. The heating from *T1*=20,5°C to *T1*=50°C took 6306 seconds and temperature difference *dT* reached 6.03°C.

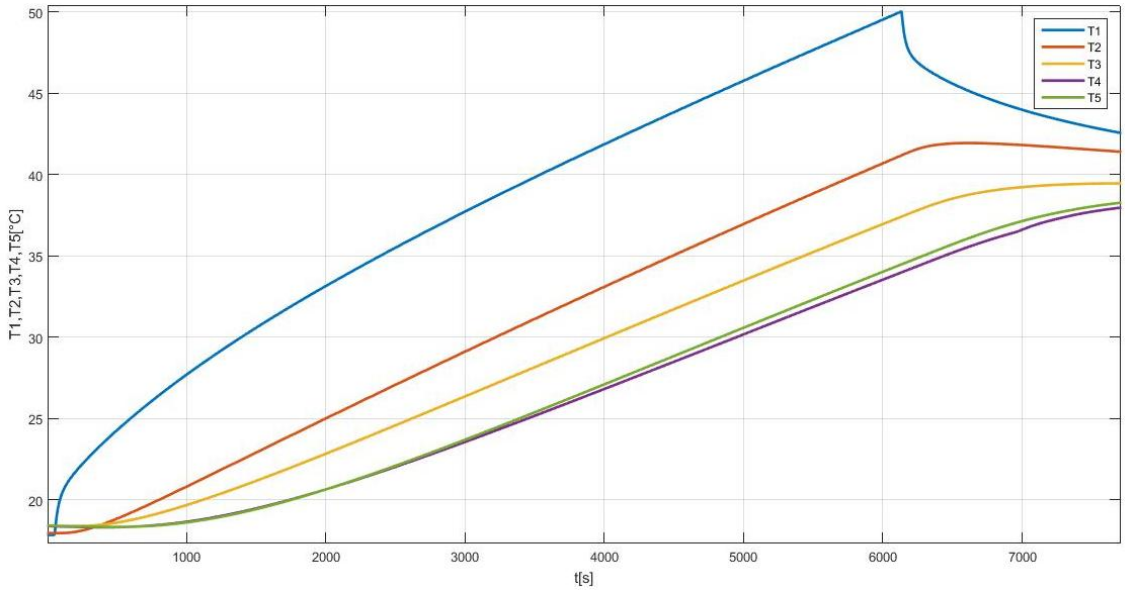

Fig. 4.3: Temperatures measured on MRW35-V1 with heat rate set to 10W

4.2.2 MRW35-V3

The heat rate during this measurement was the same as in previous one, 10W. Heating from *T1*=23.1°C to *T1*=50°C took 5,709 seconds and temperature difference *dT* reached 5.88°C. The measured temperatures are shown in Fig. 4.4.

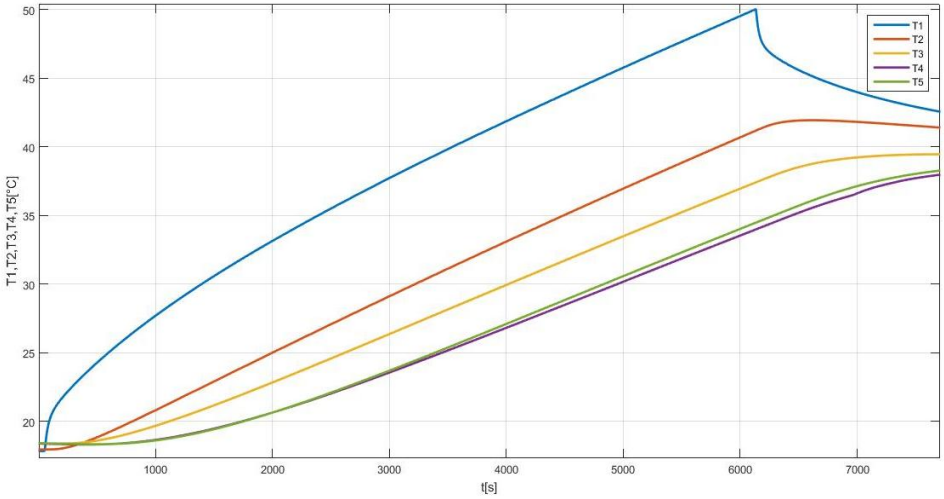

Fig. 4.4: Temperatures measured on MRW35-V3 with heat rate set to 10W

To better illustrate the differences between both measurements, temperature differences *dT* are compared with each other in Figure 4.5. It is apparent that in the case of lighter preload guideway V1, the temperature difference *dT* reaches a higher value than in the case of higher preload V3 (by 0.15°C). This fact corresponds with the idea that higher contact pressure enlarges contact area, which results in better heat conductivity. However, the difference is minimal and is smaller than uncertainty of measurement.

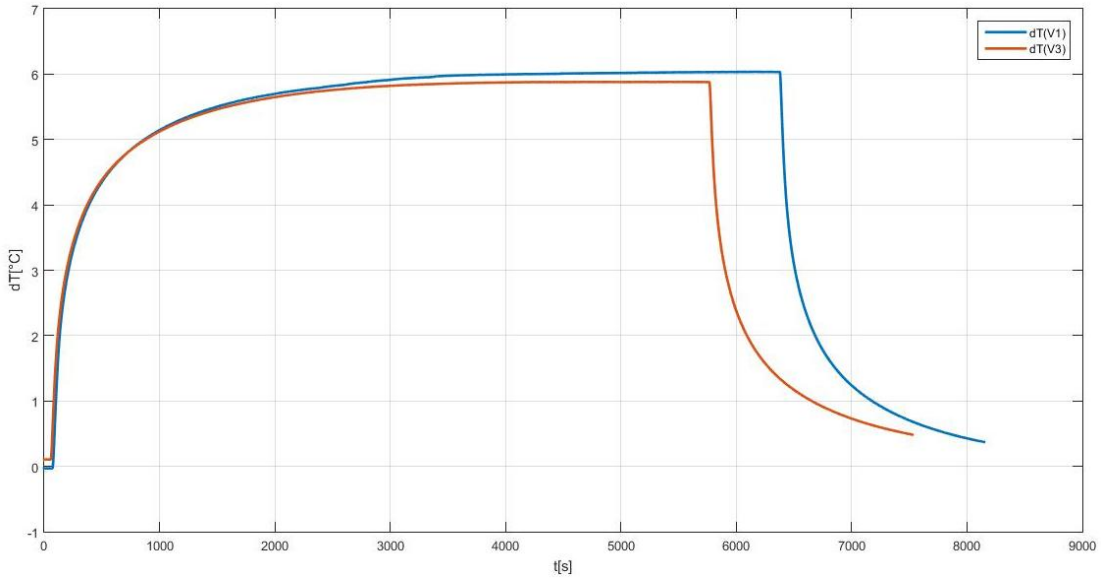

Fig. 4.5: Comparison of temperature differences dT from measurement on MRW35-V1 and MRW35-V3

4.3 Linear guideway SCHNEEBERGER MRW45-V3 (rollers rolling elements)

This type of guideway was measured two times, with different values of heat rate. The first measurement was done with heat rate set to 10W, and the second measurement with heat rate set to 15W. Both measurements are compared in Figure 4.6.

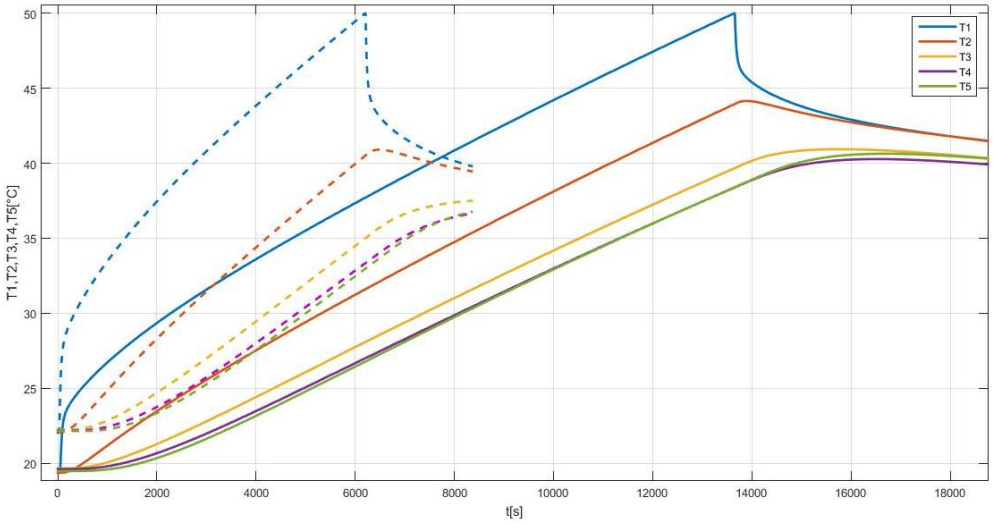

Fig. 4.6: Comparison of measurements done on guideway MRW45-V3 with different heat rates. Dashed lines stand for heat rate set to 15W, solid lines for heat rate set to 10W.

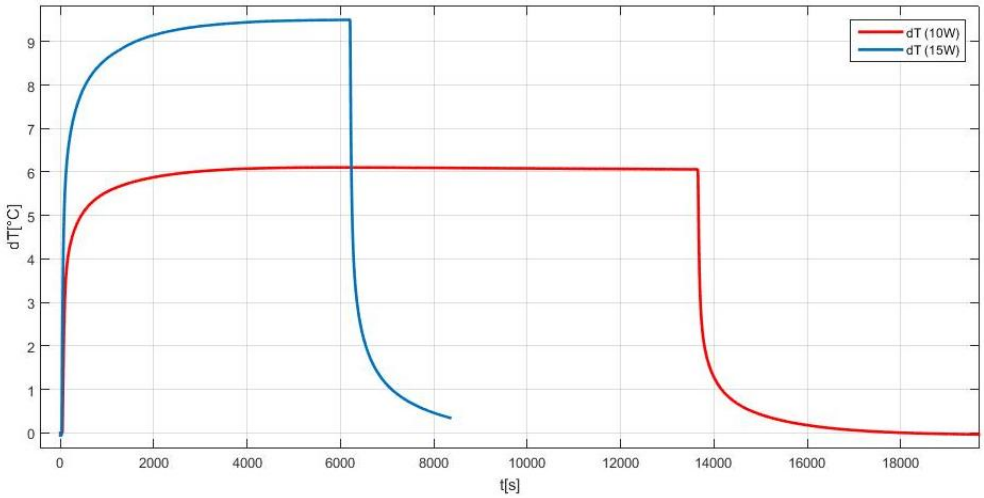

Fig. 4.7: Comparison of temperature differences measured on guideway MRW45-V3 with different heat rates.

The measurement with heat rate set to 15W started on temperature *T1*=22°C and the heating to temperature *T1*=50°C took 6,175 seconds. Temperature difference *dT* reached 9.5°C. In the measurement with heat rate set to 10W, the heating from

T1=19.4°C to *T1*=50°C took 13,608 seconds. The temperature difference reached 6.1°C and can be considered constant since approximately 4,000 seconds. It is also noticeable that in the measurement with lower heat rate the heat transfers more along the rail, as the measurement takes longer time (see temperatures *T3*, *T4* and *T5* in Fig.4.6.). Comparison of temperature differences *dT* is illustrated in Figure 4.7. It can be seen that with higher heat rate the temperature difference *dT* reaches higher value, as was expected.

4.4 Linear guideway SCHNEEBERGER MRW55-V3 (rollers rolling elements)

This type is measured as another size variation of roller guideway. Two measurements were done with heat rate set to 10W and 15W. Measured temperatures from both measurements are pictured in Figure 4.8. For the heat rate set to 15W, heating from *T1*=20.4°C to *T1*=50°C took 11,686 seconds and temperature difference *dT* reached 8.6°C. In the case of heat rate set to 10W, the heating was started at *T1*=17.8°C and was stopped at *T1*=35°C, because the temperature difference *dT* was already in steady state. It has reached 5.59°C and the heating took 9,694 seconds.

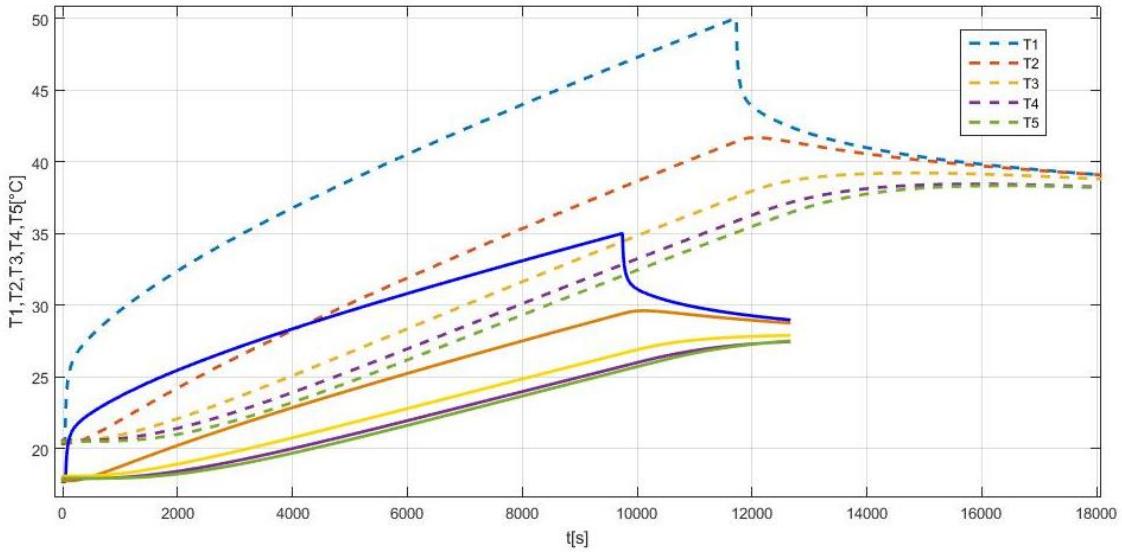

Fig. 4.8: Temperatures measured on MRW55-V3. Dashed lines stand for heat rate set to 15W, solid lines for heat rate 10W.

Temperature differences *dT* from both measurements are compared in Figure 4.9. It can be seen that *dT* reached steady state value at approximately 6,000 seconds. Further heating of the measured system is only increasing temperatures, the temperature difference *dT* remains constant.

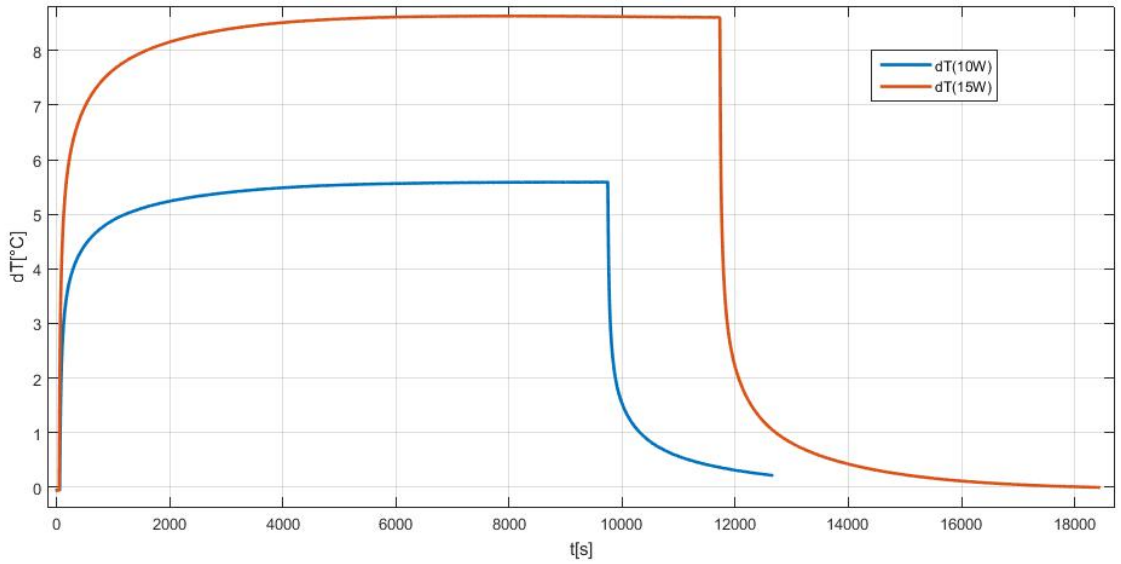

Fig. 4.9: Comparison of temperature differences measured on guideway MRW55-V3 with different heat rates.

4.5 Linear guideway SCHNEEBERGER MRW65-V3 (rollers rolling elements)

This is the largest type of guideway that was measured. Measured temperatures with heat rate set to 20W are pictured in Figure 4.10. Heating from *T1*=20.5°C to *T1*=50°C took 14,681 seconds and temperature difference *dT* reached 10.42°C. Temperature difference *dT* is pictured separately in Figure 4.11.

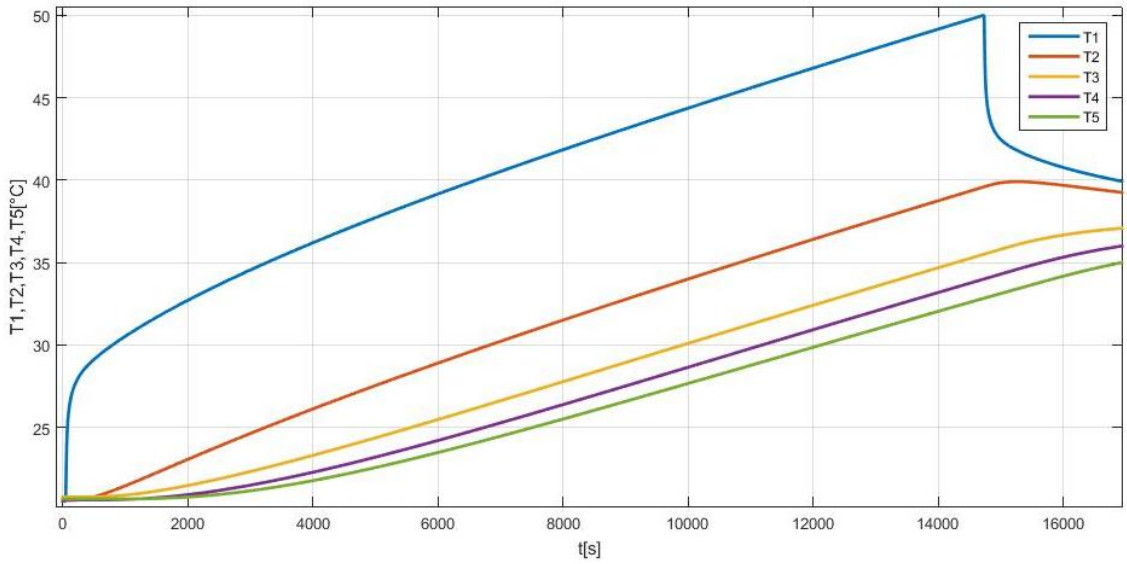

Fig. 4.10: Temperatures measured on linear guide MRW65-V3 with heat rate set to 20W

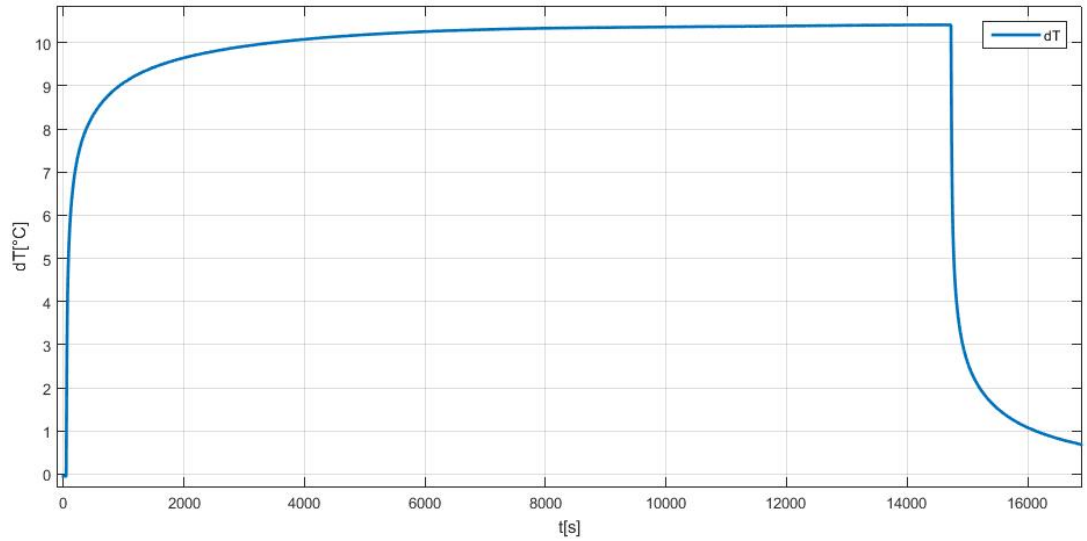

Fig. 4.11: Temperature difference dT measured on linear guide MRW65-V3 with heat rate set to 20W

4.6 Guideway SCHNEEBREGER BMW35 (balls rolling elements)

Two types of this guideway differing in size of preload were measured. The lighter class signed V1 and heavier class signed V3. Comparing these two types should show dependency of thermal resistance on the size of preload in the case of ball linear guides. Comparing this ball type of guideway with roller type MRW35 that was measured in chapter 4.2 should show the influence of the type of rolling elements on thermal resistance of linear guide.

4.6.1 BMW35-V1

Figure 4.12 shows measured temperatures. The heat rate during this test was set to 10W. Heating from *T1*=17.9°C to *T1*=50°C took 6,080 seconds and temperature difference *dT* reached 8.85°C. A detailed graph of the temperature difference *dT* is pictured together with *dT* from measurement with higher preload in Fig. 4.14.

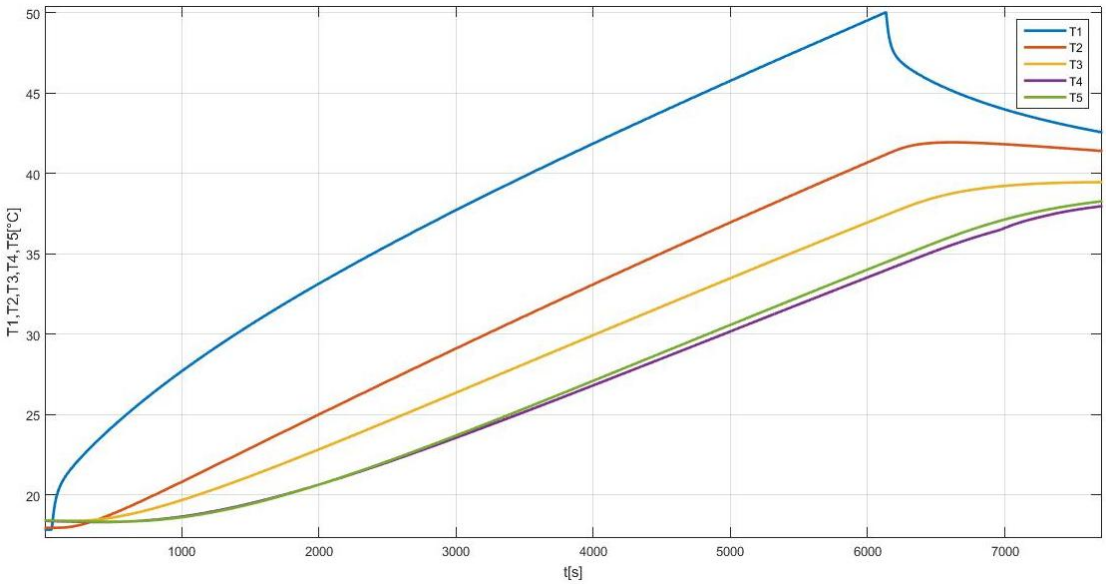

Fig. 4.12: Temperatures measured on linear guide BMW35-V1 with heat rate set to 10W

4.6.2 BMW35-V3

Heat rate during this measurement was again set to 10W. Heating from *T1*=20.8°C to *T1*=50°C took 5,531 seconds and the temperature difference *dT* reached 7.94°C. The measured temperatures are pictured in Figure 4.13.

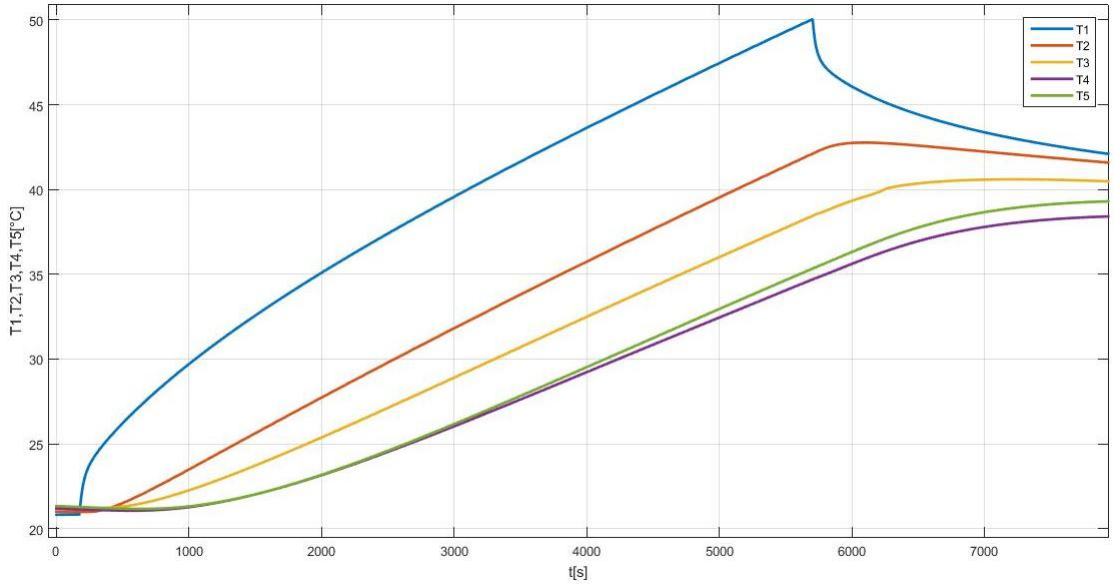

Fig. 4.13: Temperatures measured on linear guide BMW35-V3 with heat rate set to 10W

Comparison of the temperature differences *dT* from the measurement on both preload classes of guideway BMW35 can be seen in picture 4.14. The influence of preload on thermal resistance in the case of the ball guideway is more significant than in the case of the roller guideway (see Fig.4.5. for comparison).

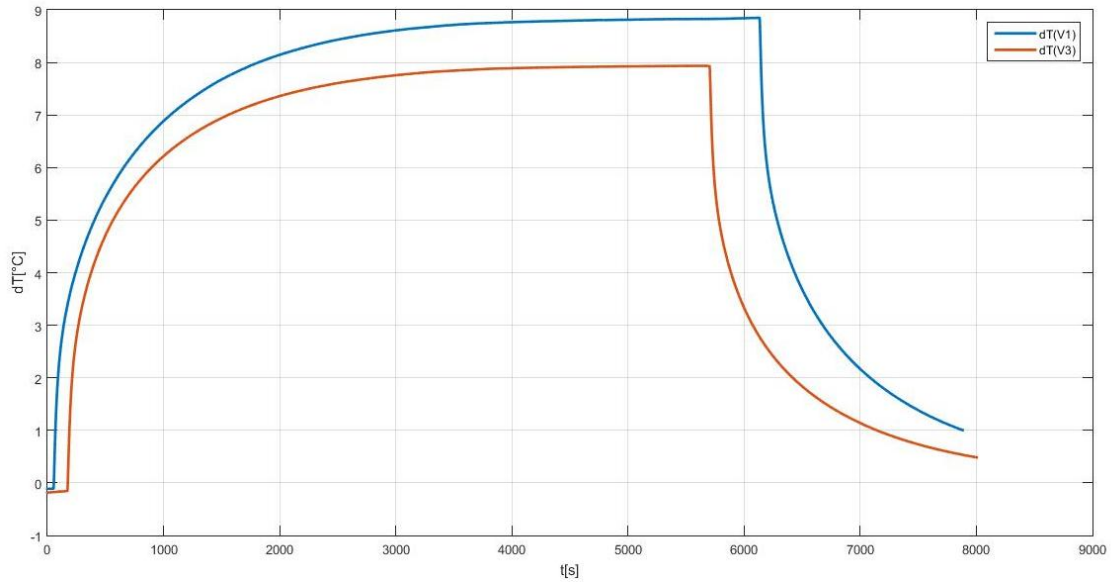

Fig. 4.14: Comparison of temperature differences dT from measurement on BMW35-V1 and BMW35-V3

5 Determination of thermal resistances across linear guideways

In this chapter, measurements results are evaluated. Firstly, chapter 5.1 states thermal resistances of measured guideways as a whole. In chapter 5.2 thermal contact resistances of rolling elements in guideways are evaluated.

5.1 Evaluation of thermal resistances of guideways

This chapter sums up measurement results and evaluates values of thermal resistances. Firstly, it compares results from a thesis [10]. It also states the influence of preload, type of rolling elements and size of linear guideway on thermal resistance.

The thermal resistances in this chapter are calculated according to equation (2.7) stated in chapter 2.5, as a ratio between temperature difference *dT* and heat rate *q*.

5.1.1 Influence of experimental setup

In chapter 4.1, results of two measurements with a different setup, but the same guideway (SCHNEEBERGER BMC30 with balls rolling elements) and same heat rate are stated.

In the experiment proposed in this thesis, with thermal insulation, the temperature difference *dT* is considered to reach steady state at 21.5°C with heat rate set to 15W. Thermal resistance is then given by:

$$R_T = \frac{dT}{q} = \frac{21.5}{15} = 1.43 \ \frac{^\circ C}{W} \tag{5.1}$$

In measurement in the thesis [10], where the guideway was placed on the base plate, the temperature difference reached steady state at 19.9°C, when heat rate was also set to 15W. Thermal resistance is then given by:

$$R_T = \frac{dT}{q} = \frac{19.9}{15} = 1.33 \ \frac{^\circ C}{W} \tag{5.2}$$

From the results it is apparent that both experiments are not completely equivalent. The value of thermal resistance in the experiment with insulation appears $0.1\frac{^\circ C}{W}$ greater than in the experiment without insulation. This can be caused by the fact

that without insulation the heat losses to the surroundings are greater than in the experiment with insulation; therefore, the real heat rate is smaller than 15W.

5.1.2 Influence of preload

The influence of preload is investigated separately for linear guideways with rollers and with balls.

5.1.2.1 Roller guideways

Results of measurements done on roller guideways MRW35, only differing in size of preload, are stated in chapter 4.2. Both measurements were done with 10W.

The temperature difference *dT* on the guideway with lighter preload V1 reached steady state at 6.03°C. The thermal resistance is given by:

$$R_T = \frac{dT}{q} = \frac{6.03}{10} = 0.6\ \frac{^\circ C}{W} \tag{5.3}$$

On the guideway with higher preload class V3, the temperature difference reached steady state at 5.88°C. The thermal resistance can be calculated:

$$R_T = \frac{dT}{q} = \frac{5.88}{10} = 0.59\ \frac{^\circ C}{W} \tag{5.2}$$

Comparing these two results, we can say that the influence of preload on thermal resistance of roller guideways is minimal and can be neglected for purposes of modeling. The results are pictured in Figure 5.1.

5.1.2.2 Ball guideways

Chapter 4.6 describes results of measurements that were done on two types of ball guideways BMW35 with different preload classes. Measurements were done with heat rate set to 10W.

The temperature difference in measurement with the lighter preload class guideway V1 reached 8.85°C. Thermal resistance is given by:

$$R_T = \frac{dT}{q} = \frac{8.85}{10} = 0.89\ \frac{^\circ C}{W} \tag{5.3}$$

In the measurement with higher preload class V3, the temperature difference *dT* reached 7.94°C. Thermal resistance is again given by:

$$R_T = \frac{dT}{q} = \frac{7.94}{10} = 0.79 \ \frac{^\circ C}{W} \tag{5.4}$$

The results of ball guideways are compared with the results of roller guideway in Figure 5.1.

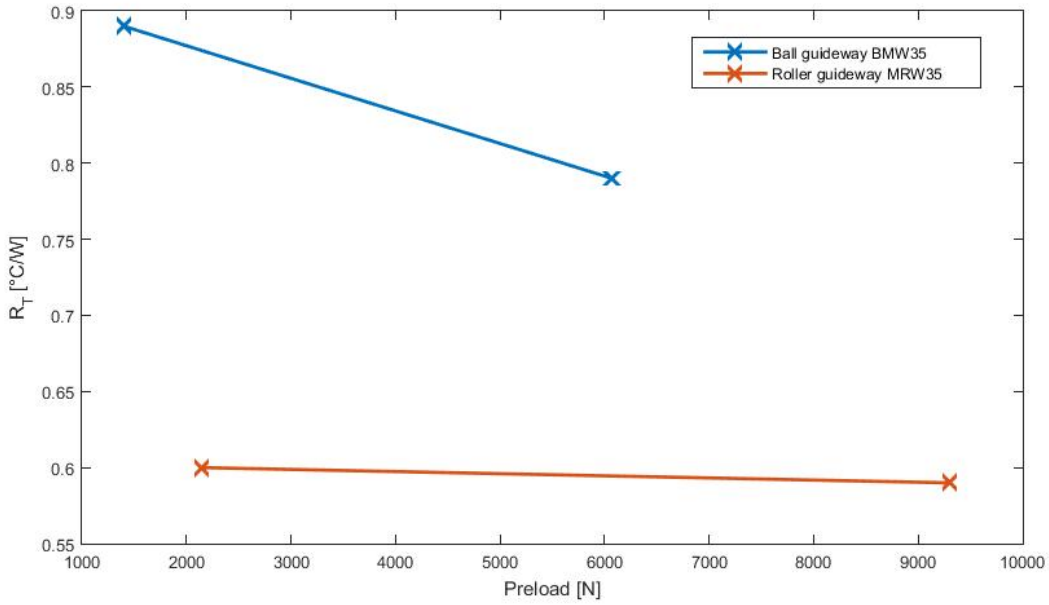

Fig. 5.1: Influence of preload on thermal resistance of linear guideways

It is apparent that in the case of the ball guideway the preload has a bigger influence on thermal resistance than in the case of the roller guideway. As was expected, the thermal resistance decreases with increasing preload. As a consequence this preload enlarges the contact area between the rolling elements and rail/carriage.

5.1.3 Influence of type of rolling element

From the results in the previous chapter, we can also evaluate the influence of the type of rolling elements on thermal resistance.

If we compare the lighter preload classes V1, the thermal resistance is 0.89 $\frac{^\circ C}{W}$ for the ball type guideway and 0.6 $\frac{^\circ C}{W}$ for the roller type guideway. The influence will be smaller if we compare the higher preload class V3 - the ball guideway has thermal resistance 0.79 $\frac{^\circ C}{W}$ and the roller guideway 0.59 $\frac{^\circ C}{W}$.

However the difference of thermal resistance between ball and roller type of guideways is not negligible and should be considered in modeling. The results correspond with our expectations as the contact area of rollers is larger than the contact area of balls (line contact versus point contact).

5.1.4 Influence of linear guideways size

This chapter sums up measurements that were done on different sizes of roller guideway MRW and evaluates values of thermal resistances.

Fig. 5.2 shows temperature differences measured on guideway MRW with differing size from 35 to 55 with heat rate set to 10W. Size 65 was also measured, but with heat rate set to 20W, so the temperature difference should be two times bigger than with heat rate set to 10W. For better illustration the temperature difference from measurement on MRW65 was divided by two.

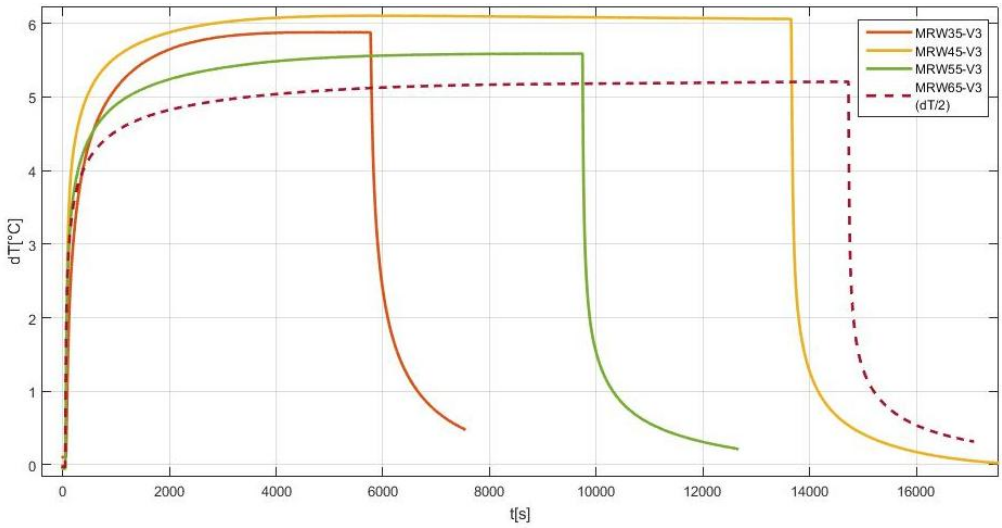

Fig. 5.2: Comparison of measured temperature differences on linear guideways differing in size

From Fig.5.2 we can read the temperature differences in steady state and then calculate thermal resistance according to equation (2.7). Results from all measurements that were done on size variations of the MRW type of guideway with the highest class of preload V3 is summarized in Table 5.1 and graphically presented in Figure 5.3.

	q [W]	dT [°C]	R_T [°C/W]
MRW35 V3	10	5.88	0.59
MRW45 V3	10	6.1	0.61
MRW45 V3	15	9.5	0.63
MRW55 V3	10	5.59	0.56
MRW55 V3	15	8.6	0.57
MRW65 V3	20	10.42	0.52

Tab. 5.1: Thermal resistances of guideways differing in size

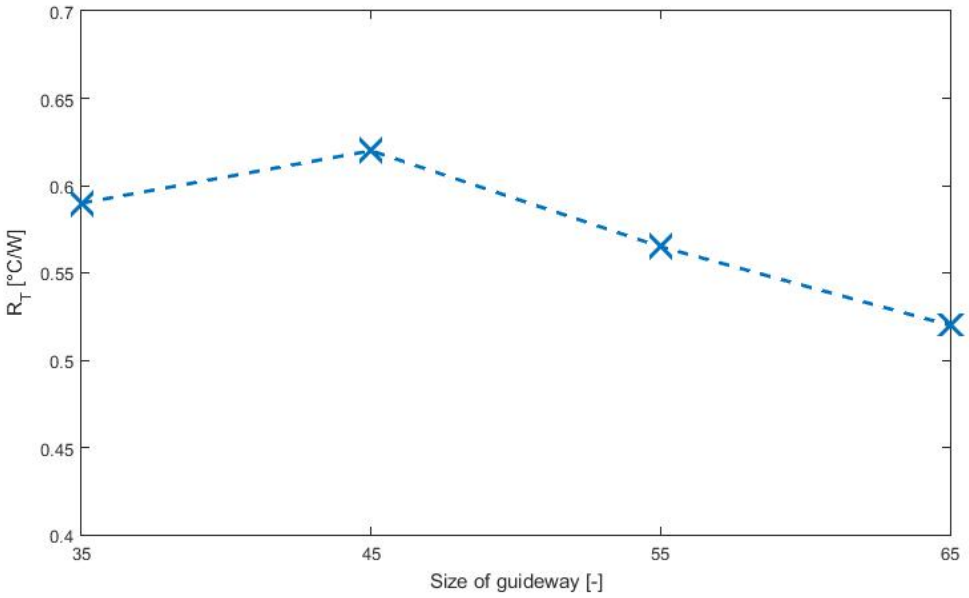

Fig. 5.3: Influence of size of MRW guideway on its thermal resistance

From the results above it can be concluded that the size of guideway does not have a significant influence on its thermal resistance. The highest thermal resistance was measured on the guideway of size 45 and the lowest on the guideway of size 65 while these two values are differing by only 0.1°C/W.

5.2 Evaluation of thermal contact resistance in guideways

In this chapter an estimation of thermal contact resistance of rolling elements in guideways is stated.

5.2.1 Theoretical background

This chapter states equations describing behavior of heat transfer across discrete system with *n* degrees of freedom. Basic equation can be expressed as:

$$[M]\left\{\frac{dT}{dt}\right\} + [K]\{T(t)\} = \{Q(t)\} \tag{5.5}$$

where $[M]$ is thermal inertia matrix, $[K]$ is thermal conductivity matrix and $\{Q(t)\}$ is thermal exciting vector. It is a system of *n* first order linear differential equations with constant coefficients. So, the general solution of the system will be the sum of the general solution of homogeneous system plus a particular solution of the whole system (5.5) [17].

The homogeneous system is:

$$[M]\left\{\frac{dT}{dt}\right\} + [K]\{T(t)\} = \{0\} \tag{5.6}$$

Following possible solutions can be tried out:

$$\{T(t)\} = \{V\}e^{-\lambda t}\ ;\ \left\{\frac{dT}{dt}\right\} = -\lambda\{V\}e^{-\lambda t} \tag{5.7}$$

Replacing in homogeneous system (5.6) results:

$$([K] - \lambda[M])\{V\} = \{0\} \tag{5.8}$$

System (5.8) is generalised problem of eigenvalues and eigenvectors. By simple edit we receive:

$$[K]\{V_i\} = \lambda_i[M]\{V_i\} \tag{5.9}$$

where λ_i is the eigenvalue number *i* and $\{V_i\}$ is the associated eigenvector.

As it is known, eigenvectors are orthogonal with respect to matrix $[K]$ and $[M]$:

$$\{V_i\}^T[M]\{V_j\} = 0; \{V_i\}^T[K]\{V_j\} = 0;\ \ \forall i \neq j \tag{5.10}$$

It will be assumed that eigenvectors $\{V_i\}$ are normalized in relation to $[M]$ matrix:

$$\{V_i\}^T[M]\{V_i\} = 1 \quad \forall i \tag{5.11}$$

From the expressions (5.9), (5.10) and (5.11) can be deduced easily the following expression:

$$\{V_i\}^T[K]\{V_i\} = \lambda_i \quad \forall i \tag{5.12}$$

They are defined: *[V]* is a matrix which columns are the eigenvectors normalized respect to thermal inertia matrix, *[λ]*is a diagonal matrix which elements are the eigenvalues and *[I]* is the usual identity matrix [17].

From (5.10) to (5.12) expressions it can be deduced:

$$[V]^T[M][V] = [I] \tag{5.13}$$

$$[V]^T[K][V] = [\lambda] \tag{5.14}$$

From expression (5.9) it is obtained:

$$[K][V] = [M][V][\lambda] \tag{5.15}$$

The eigenvectors $\{V_i\}$ form a system of *n* linearly independent vectors that constitute a base. The temperature vector $\{T(t)\}$ can be expressed related to this base with some new coordinates $x_i(t)$*[17]*.

$$\{T(t)\} = \sum_{i=1}^{n}\{V_i\}x_i(t) \tag{5.16}$$

Expressing (5.16) in matrix form:

$$\{T(t)\} = [V]\{x_i(t)\} \tag{5.17}$$

The derivate of expression (5.17) is:

$$\left\{\frac{dT}{dt}\right\} = [V]\left\{\frac{dx}{dt}\right\} \tag{5.18}$$

Replacing (5.17) and (5.18) in system (5.5):

$$[M][V]\left\{\frac{dx}{dt}\right\} + [K][V]\{x(t)\} = \{Q(t)\} \tag{5.19}$$

Multiplying (5.19) by $[V]^T$:

$$[V]^T[M][V]\left\{\frac{dx}{dt}\right\} + [V]^T[K][V]\{x(t)\} = [V]^T\{Q(t)\} \tag{5.20}$$

Following vector is defined:

$$\{\phi(t)\} = [V]^T\{Q(t)\} \tag{5.21}$$

being:

$$\phi_i(t) = \{V_i\}^T\{Q(t)\} \tag{5.22}$$

Replacing (5.13), (5.14) and (5.21) in expression (5.20) it results:

$$\left\{\frac{dx}{dt}\right\} + [\lambda]\{x(t)\} = \{\phi(t)\} \tag{5.23}$$

Because of $[\lambda]$ is a diagonal matrix, it can be seen that (5.23) is a system of *n* uncoupled equations like the following:

$$\frac{dx_i}{dt} + \lambda_i x_i(t) = \phi_i(t) \tag{5.24}$$

So, with $\{x(t)\}$ coordinates, called natural coordinates, the system of *n* differential equations with *n* variables becomes *n* equations of a single variable. The eigenvectors $\{V_i\}$ are called natural thermal modes, and the methodology employed for uncoupling equations of thermal balance is called modal analysis. The previous theoretical development demonstrates that the temperature in each point of a machine working under fixed conditions can be expressed like a linear combination of a series of exponential time functions. Furthermore the time constants of the exponentials are common for all the points whose temperatures are analyzed. The experimental thermal modal analysis consists on fitting the coefficients and exponents of the mentioned exponential expressions for adapting them to the measured experimental data [17].

5.2.2 Estimation of thermal contact resistance

For the purpose of estimation of thermal contact resistance of measured linear guideways, a script in Matlab was developed. The script is based on experimental thermal modal analysis, which consists on fitting the coefficients and exponents of exponential expressions for adapting them to the measured data as was described in 5.2.1. The script can be found in Appendix C.

The measured assembly is modeled by a one-dimensional model that is described in figure 5.4.

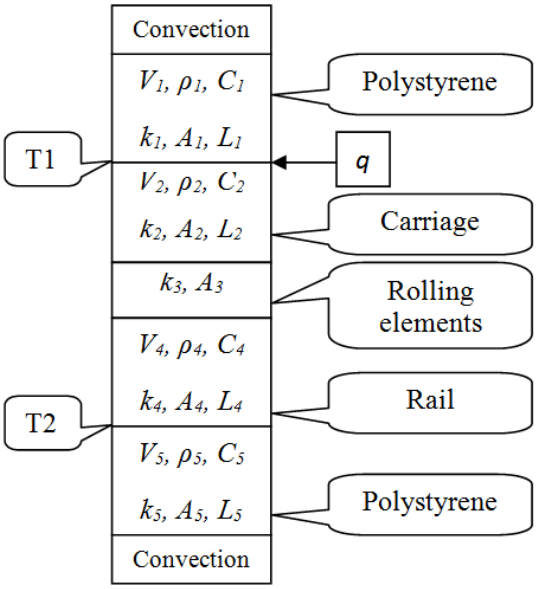

Fig. 5.4: One-dimensional model for estimating thermal contact resistance in guideways

The material properties of polystyrene, carriages and rails are stated in chapter 3 and their volumes V are differing with type and size and were determined based on CAD models. Specific values can be found in Electronic appendix.

For the estimation of thermal contact resistance, the measured temperatures *T1* and *T2* of all guideways are fitted with the mathematical model. The main estimated parameter for fitting the modeled curves at the measured curves is the parameter of conductivity of the contact of rolling elements K_3, that is given by:

$$K_3 = k_3 A_3 \tag{5.25}$$

From (5.25) we can easily calculate thermal contact conductance k_3:

$$k_3 = \frac{K_3}{A_3} \tag{5.26}$$

where the area of contact A_3 was determined based on CAD models for all linear guideways.

The thermal contact resistance of the rolling elements in guideways is then given by:

$$R_T^{"} = \frac{1}{k_3} \tag{5.27}$$

This method of estimation was used for all measured guideways. The graphical results of fitting can be found in Appendix B. All models were fitted to the measured temperatures *T1* and *T2* with maximum error of 1°C. The numerical results of thermal contact resistances are summarized in Table 5.2.

Guideway	Preload	A_3 [m^2]	$K_3 \left[\frac{W}{°C}\right]$	$k_3 \left[\frac{W}{°C \cdot m^2}\right]$	$R_T^{"} \left[\frac{°C \cdot m^2}{W}\right]$
BMW35	V1	$1.95 \cdot 10^{-3}$	1.0	5.133	$1.95 \cdot 10^{-3}$
	V3	$1.95 \cdot 10^{-3}$	1.1	5.647	$1.77 \cdot 10^{-3}$
MRW35	V1	$3.79 \cdot 10^{-3}$	1.7	4.489	$2.23 \cdot 10^{-3}$
	V3	$3.79 \cdot 10^{-3}$	1.8	4.753	$2.10 \cdot 10^{-3}$
MRW45	V3	$6.11 \cdot 10^{-3}$	1.9	3.110	$3.22 \cdot 10^{-3}$
MRW55	V3	$8.25 \cdot 10^{-3}$	1.8	2.182	$4.58 \cdot 10^{-3}$
MRW65	V3	$11.37 \cdot 10^{-3}$	2.2	1.935	$5.17 \cdot 10^{-3}$

Tab. 5.2: Results of estimation of thermal contact resistance

6 FE modeling based on obtained experimental data

This chapter is briefly suggesting possible use of evaluated data for FE modeling of thermal behavior of mechanical systems with linear guideways.

6.1 FE modeling of guideway as a whole

First possibility of FE modeling uses the results stated in chapter 5.1, summarized in Tab. 6.1. They can be used for thermal modeling of linear guideway as is described in Figure 5.5. In this case the whole guideway is in the thermal model substituted with one value of thermal resistance.

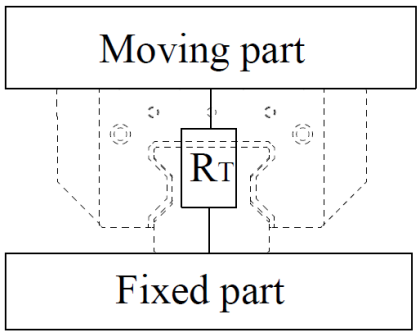

Fig. 6.1: Substitution of whole guideway with one value of thermal resistance

Guideway	*Preload*	$R_T \left[\frac{°C}{W}\right]$
BMW35	*V1*	*0.89*
	V3	*0.79*
MRW35	*V1*	*0.6*
	V3	*0.59*
MRW45	*V3*	*0.62*
MRW55	*V3*	*0.57*
MRW65	*V3*	*0.52*

Tab. 6.1: Summarized results from chapter 5.1

6.2 FE modeling of guideway with thermal contact resistance

Second option of thermal modeling of guideways uses the results from chapter 5.2, summarized in Table 5.2.

In this case, the values of thermal contact resistances $R_T^{"}$ will be applied on all 4 areas of contact between the carriage and the rail (area A_3 in Table 5.2). This option is pictured in Figure 6.2.

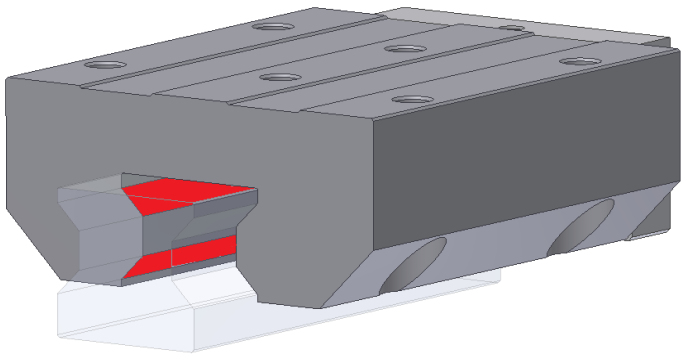

Fig. 6.2: FE modeling of thermal behavior of guideway with values of thermal contact resistance

7 Conclusion

The aim of work was to experimentally determine thermal resistances of different types of rolling linear guideways and to investigate the influence of preload, type of rolling elements and size of guideway on its thermal resistance.

Theoretical part of this work firstly describes basic types of linear guideways used in machine tool design. Then it concentrates on measuring of temperature, types of thermometers and their principles. It also states basic types of heat transfer and defines quantities that describe it. Chapter 2.6 is deduced to the empirical models of thermal contact conductance and then an example of heat transfer across bolted joints as a typical machine part is described. Last chapters of theoretical part states some experiments for determining thermal resistance and other experiments that deal with thermo-mechanical properties of linear guideways.

For the determination of thermal resistances of linear guideways an experiment was proposed and several measurements with different types of guideways were executed. Results of measurements are stated in chapter 4 and then evaluated in chapter 5.

Firstly a measurement on the guideway that was measured in thesis [10] was executed. Result is used for comparison of the value of thermal resistance with different experimental set up. The values of thermal resistance from both set ups are differing by 0.1 °C/W.

The evaluated values of thermal resistances of different types of guideways are summarized in Table 7.1. The first type of evaluation is determining thermal resistance R_T of the guideway as a whole and influence of parameters on the thermal resistance is investigated. Influence of preload on thermal resistance in the case of ball guideways is more significant than in the case of roller guideways. Chapter 5.3 states the influence of the type of rolling elements on thermal resistance comparing the results from ball guideways with roller guideways. The influence is not negligible and should be considered in FE modeling. The last influencing parameter that was investigated is the size of guideway. This parameter does not have significant influence on thermal resistance.

The second type of evaluation is determining the contact thermal resistance $R_T^{"}$ of the rolling elements in guideways. For that purpose a script in Matlab based on the modal analysis was written.

Guideway	Preload	$R_T \left[\frac{°C}{W}\right]$	$R_T^{"} \left[\frac{°C \cdot m^2}{W}\right]$
BMW35	V1	0.89	$1.95 \cdot 10^{-3}$
	V3	0.79	$1.77 \cdot 10^{-3}$
MRW35	V1	0.6	$2.23 \cdot 10^{-3}$
	V3	0.59	$2.10 \cdot 10^{-3}$
MRW45	V3	0.62	$3.22 \cdot 10^{-3}$
MRW55	V3	0.57	$4.58 \cdot 10^{-3}$
MRW65	V3	0.52	$5.17 \cdot 10^{-3}$

Tab. 7.1: Summarization of results

Last chapter is suggesting possible usage of evaluated values in FE modeling of linear guideways.

8 Lists

8.1 Literature

[1] BORSKÝ, V., *Základy stavby obráběcích strojů*, skriptum ES VUT, 2. vydání, Grafia Prostějov, 1991, s. 214, ISBN 80-214-0361-6.

[2] MAREK J. a kol., *Konstrukce CNC obráběcích strojů*, MM publishing, 2006, s. 420, ISBN 978-80-254-7980-3.

[3] JENČÍK J., VOLF J. a kolektiv, *Technická měření*, skriptum FS ČVUT, 1. vydání, Vydavatelství ČVUT, 2000, s. 213, ISBN 80-01-02138-6.

[4] SCHNEEBERGER Linear technology [online]. [cit. 2014-11-2]. Available at http://www.schneeberger.com

[5] National instruments [online]. [cit.2014-11-8]. Available at http://www.instrumentationtoolbox.com/

*[*6] INCROPERA, DEWITT, BERGMAN, LAVINE, *Fundamentals of heat and mass transfer*, sixth edition, Wiley, 997 pages, ISBN 0-471-76115-X.

[7]HASSELSTRÖM J., NILSSON E. *Thermal Contact Conductance in Bolted Joints.* Gothenburg: Chalmers University of Technology, 2012. Diploma work. Department of Materials and Manufacturing Technology.

[8] BAHRAMI M., CULHAM J.R., YOVANOVICH M.M., SCHNEIDER G.E., *Review of thermal joint resistance models for nonconforming rough surfaces,* University of Waterloo, Department of Mechanical Engineering, 2006.

[9] MANTELLI M., YOVANOVICH M.M., *Compact analytical model for overall thermal resistance of bolted joints,* Elsevier science ltd., 1998.

[10] ŠLINC Miroslav. *Sdílení tepla přes lineární vedení.* Praha: 2014. Diplomová práce, ČVUTv Praze, Fakulta strojní, Ústav výrobních strojů a zařízení. Vedoucí práce Ing. Otakar Horejš Ph.D.

[11] SCHOVÁNEK, Petr. *Chyby a nejistoty měření.* Univerzita Palackého v Olomouci [online]. 2007 [cit. 2015-05-12]. Available at:

http://fyzika.upol.cz/cs/system/files/download/vujtek/texty/pext2-nejistoty.pdf

[12] INNOVATIVE SENSOR TECHNOLOGY, Data sheet for *platinum temperature sensors*, [online], [cit.2015-03-15], available at http://www.ist-ag.com/

[13] BELL S., *A Beginner's Guide to Uncertainty of Measurement,* National Phzsical Laboratory: Centre for basic, Thermal and Length Metrology, 2012.

[14] *Thermal Interface Resistance Measurement – Power Electronics Application.* [online]. [cit. 2015-04-11]. Available at https://ujdigispace.uj.ac.za/bitstream/handle/10210/1739/08Chapter08.pdf?sequence=9

[15] *DMC V series* [online], DMG MORI. [cit.2015-05-14]. Available at http://cz.dmgmori.com/

[16] BREACHER C., FEZ M., NEUS S., SHNEOR Y., BAKARINOW K., *Influences on the thermal behaviour of linear guide and externally driven spindle systems,* Aachen: Aachen University, 2014.

[17] URIARTE, L., ZATARAIN, M. T*hermal modal analysis and the compensation of thermal distortions*. In: Euspen SIG Seminar 2006, Eindhoven, The Netherlands.

8.2 List of figures

8.3 List of tables

8.4 List of used software

Microsoft Office Word 2010

Microsoft Office Excel 2010

Matlab 2014a

Autodesk Inventor Professional 2013

LabVIEW 2013

8.5 Appendix list

Text appendix:

Appendix A: Outer temperatures during measurements

Appendix B: Results of fitting the mathematical model to the measured temperatures

Appendix C: Script for evaluation of thermal contact resistance of contact of rolling elements in guideways

Electronic appendix:

Electronic version of thesis

Results of measurements in text files (.lvm)

Scripts for evaluation of thermal contact resistances set up for all measured guideways

Appendix A: Outer temperatures during measurements

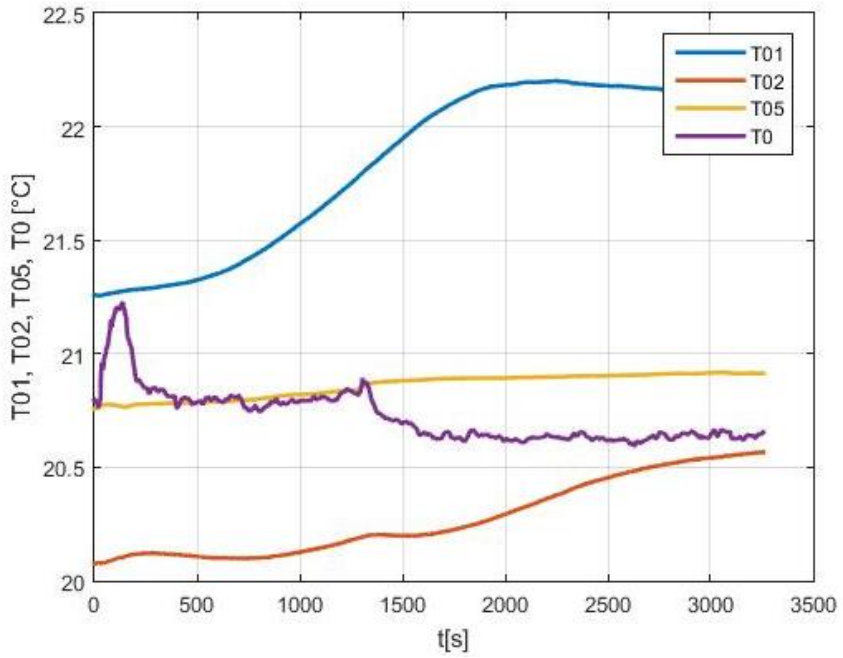

Fig. A. 1: Outer temperatures during measurement on BMC30 with heat rate set to 15W

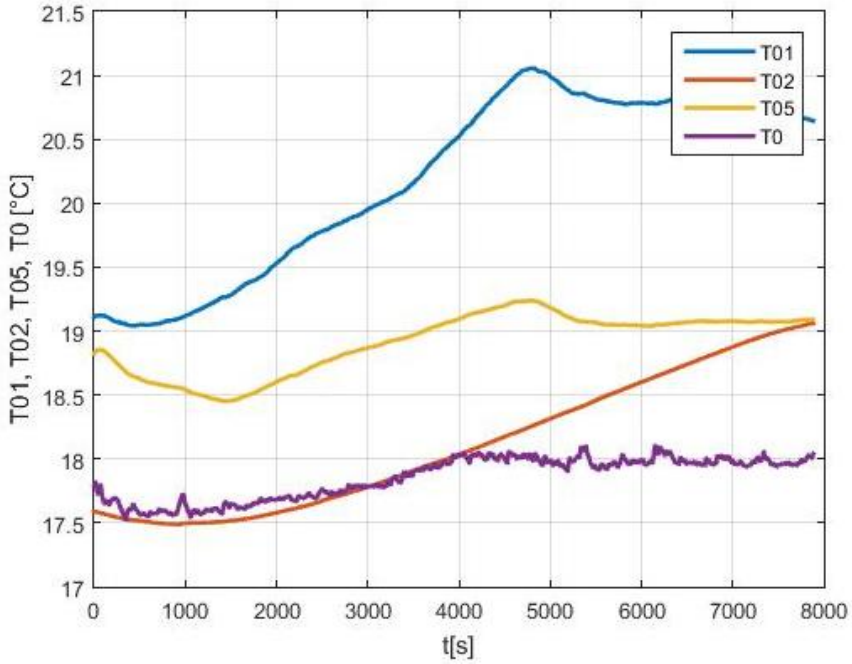

Fig. A. 2: Outer temperatures during measurement on BMV-V1 with heat rate set to 10W

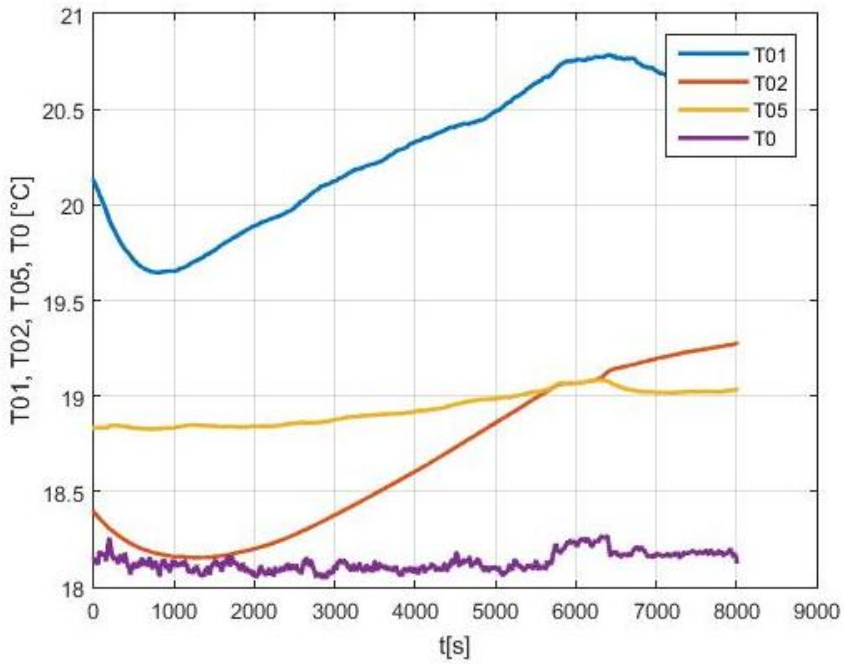

Fig. A. 3: Outer temperatures during measurement on BMV-V3 with heat rate set to 10W

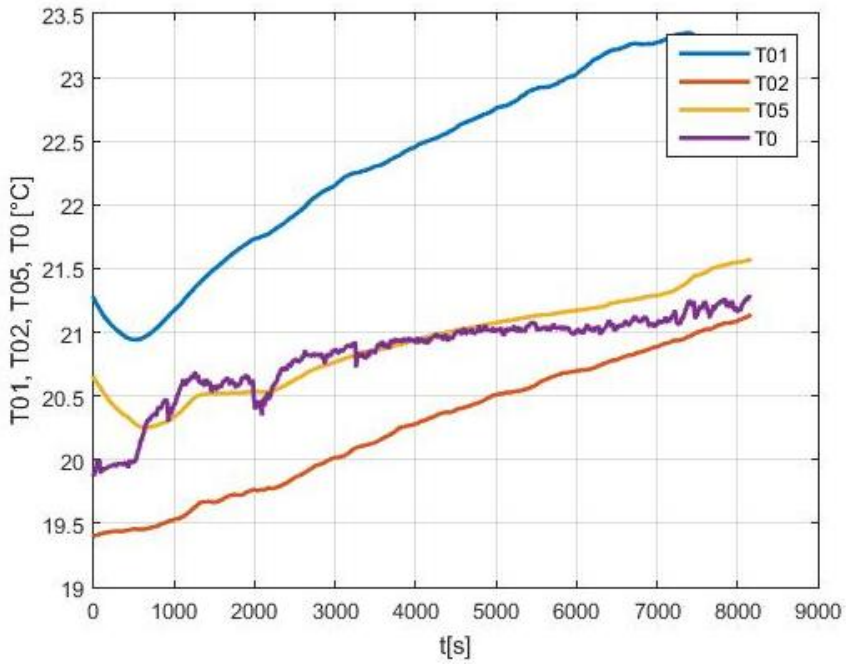

Fig. A. 4: Outer temperatures during measurement on MRW-V1 with heat rate set to 10W

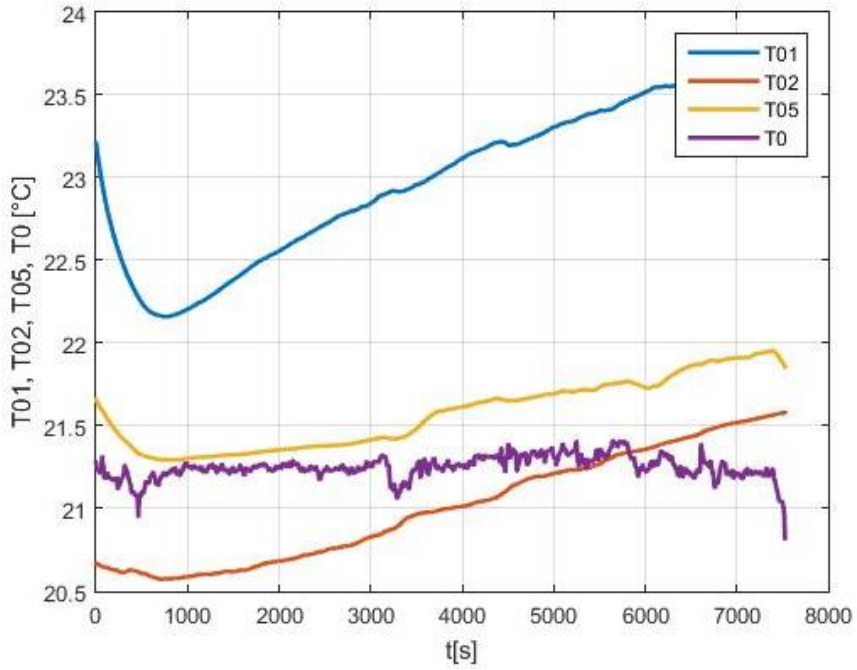

Fig. A. 5: Outer temperatures during measurement on MRW35-V3 with heat rate set to 10W

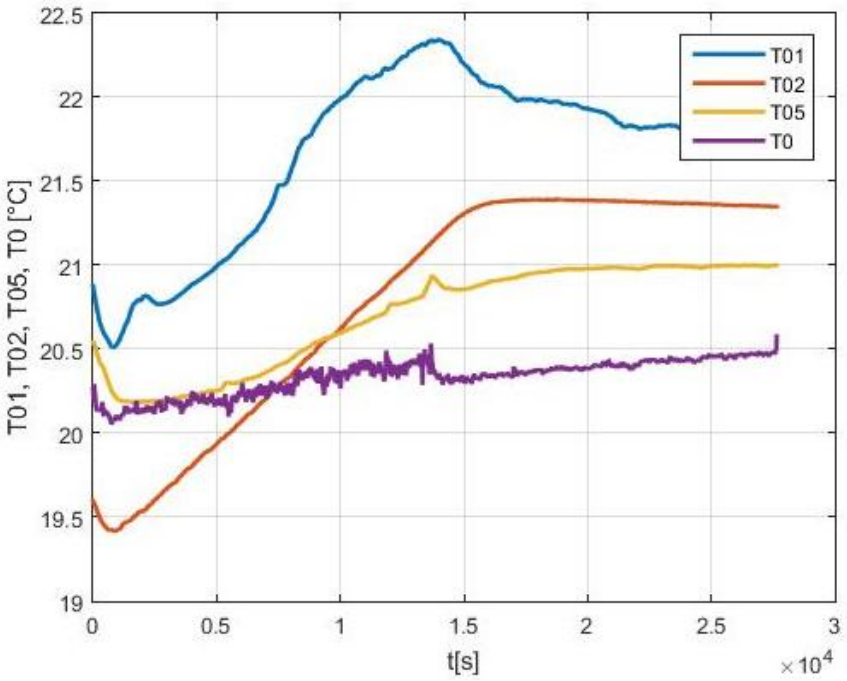

Fig. A. 6: Outer temperatures during measurement on MRW45-V3 with heat rate set to 10W

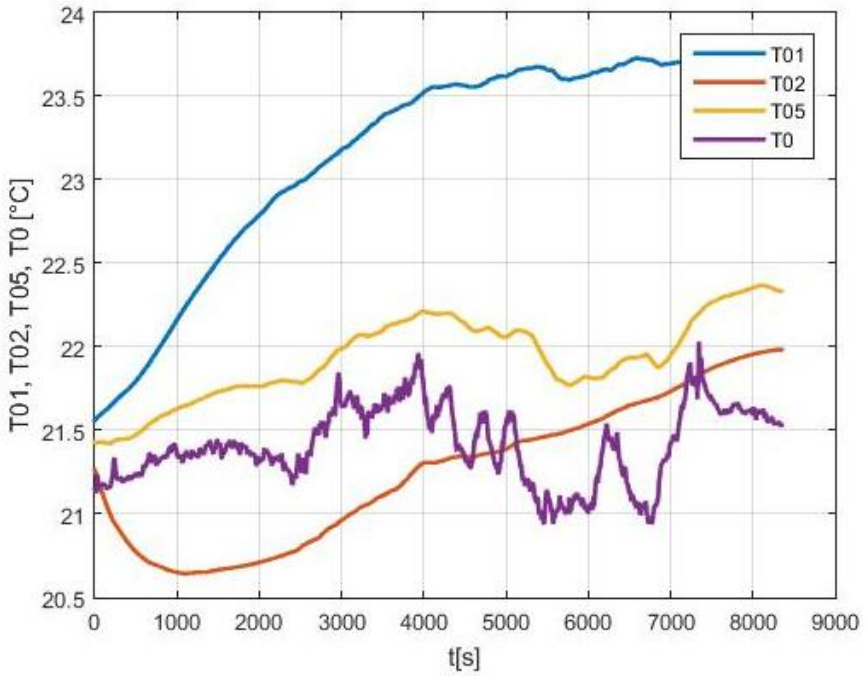

Fig. A. 7: Outer temperatures during measurement on MRW45-V3 with heat rate set to 15W

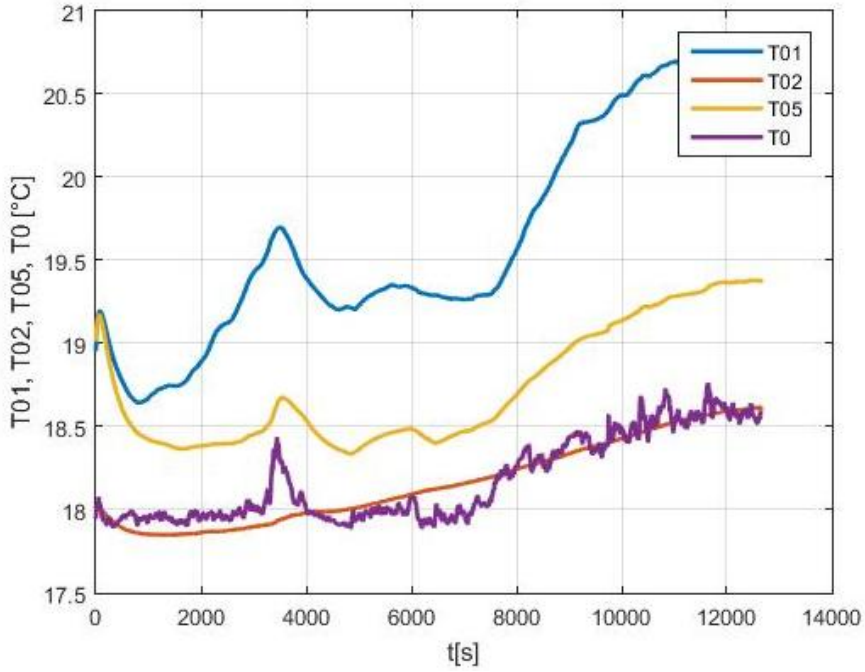

Fig. A. 8: Outer temperatures during measurement on MRW55-V3 with heat rate set to 10W

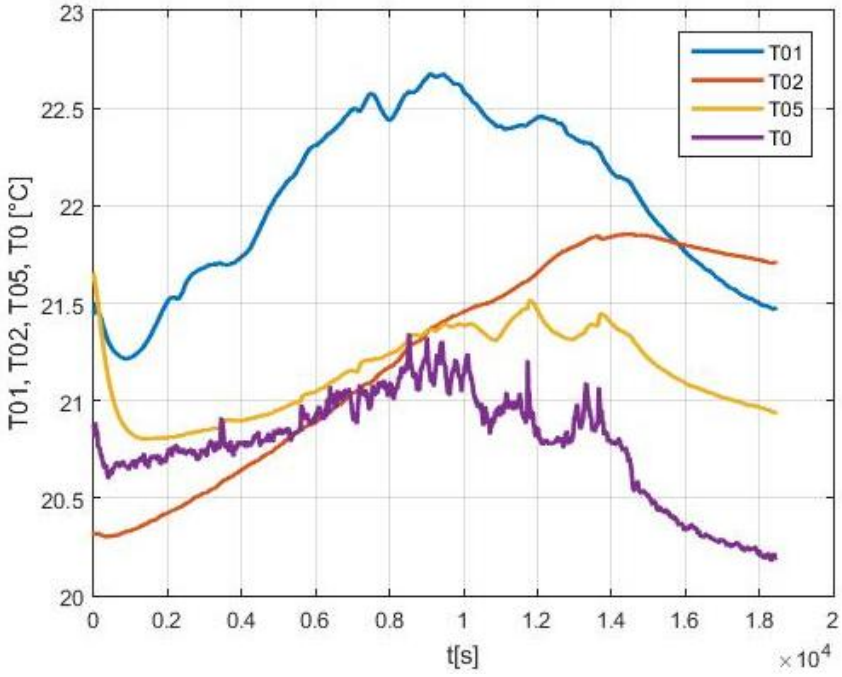

Fig. A. 9: Outer temperatures during measurement on MRW55-V3 with heat rate set to 15W

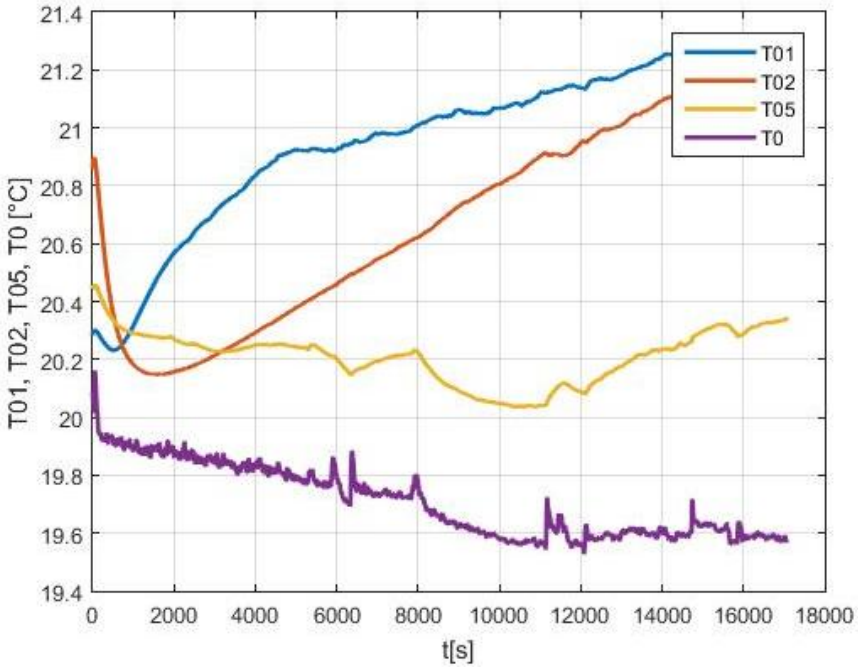

Fig. A. 10: Fig. A. 9: Outer temperatures during measurement on MRW65-V3 with heat rate set to 20W

Appendix B: Results of fitting the mathematical model to the measured temperatures

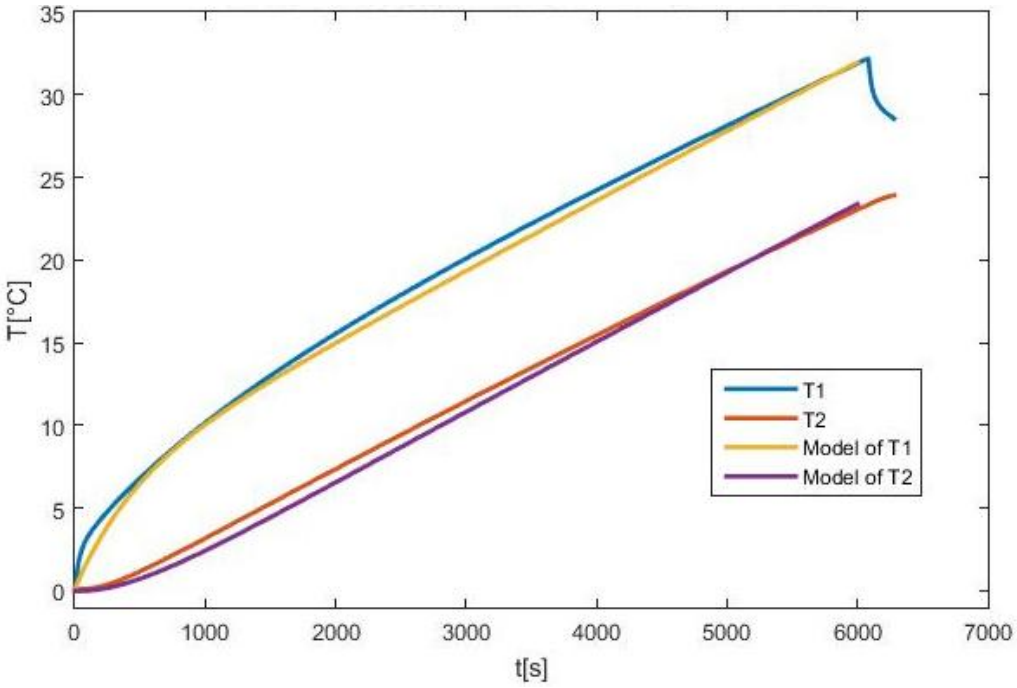

Fig. B.1: Modeled temperatures fitted to measured temperatures T1 and T2 on BMW35-V1

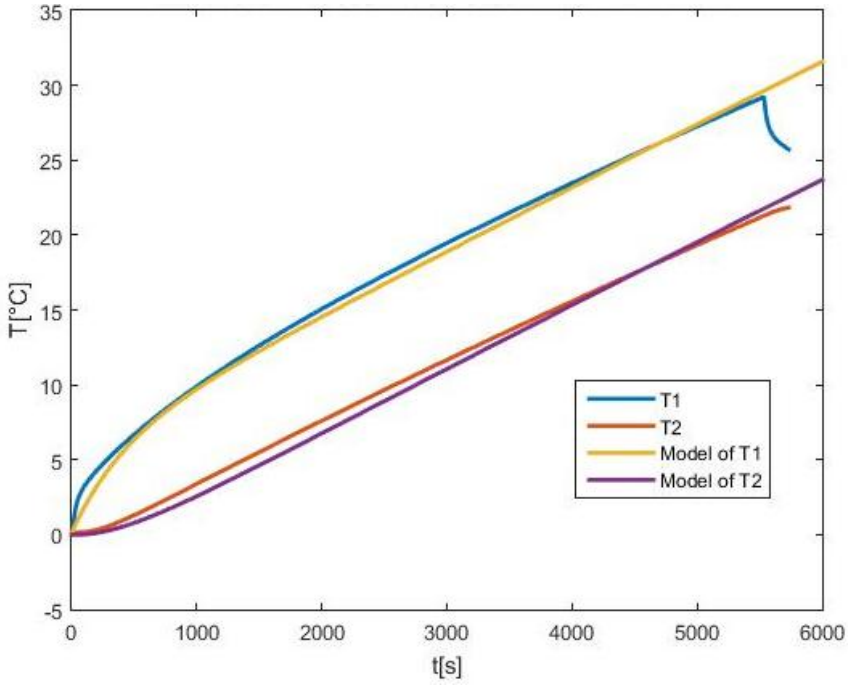

Fig. B 2: Modeled temperatures fitted to measured temperatures T1 and T2 on BMW35-V3

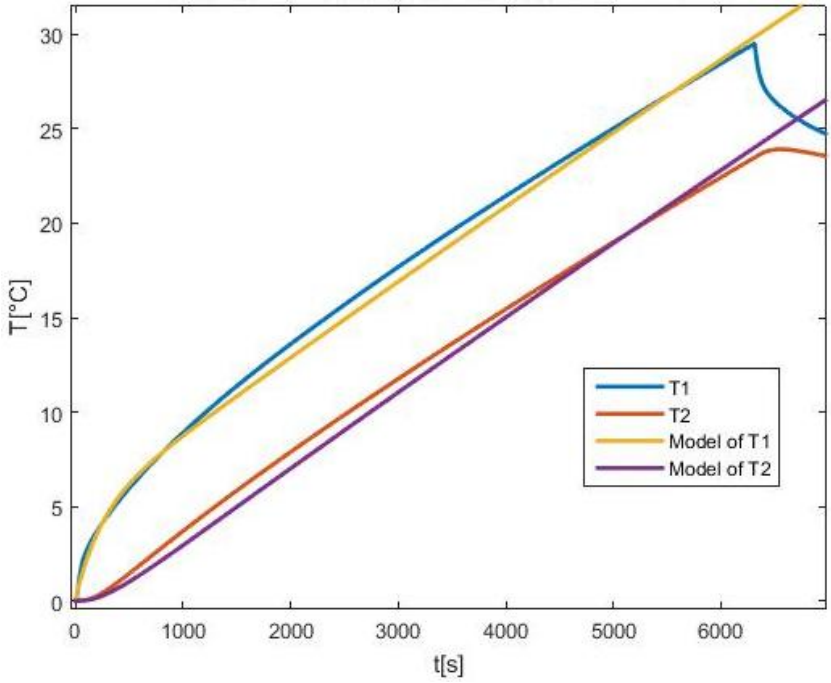

Fig. B.3: Modeled temperatures fitted to measured temperatures T1 and T2 on MRW35-V1

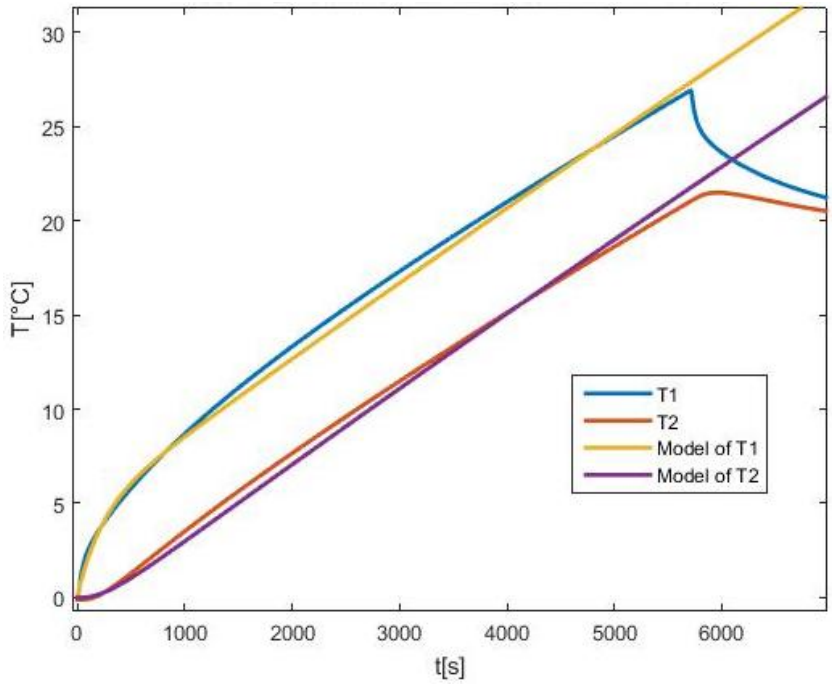

Fig. B.4: Modeled temperatures fitted to measured temperatures T1 and T2 on MRW35-V3

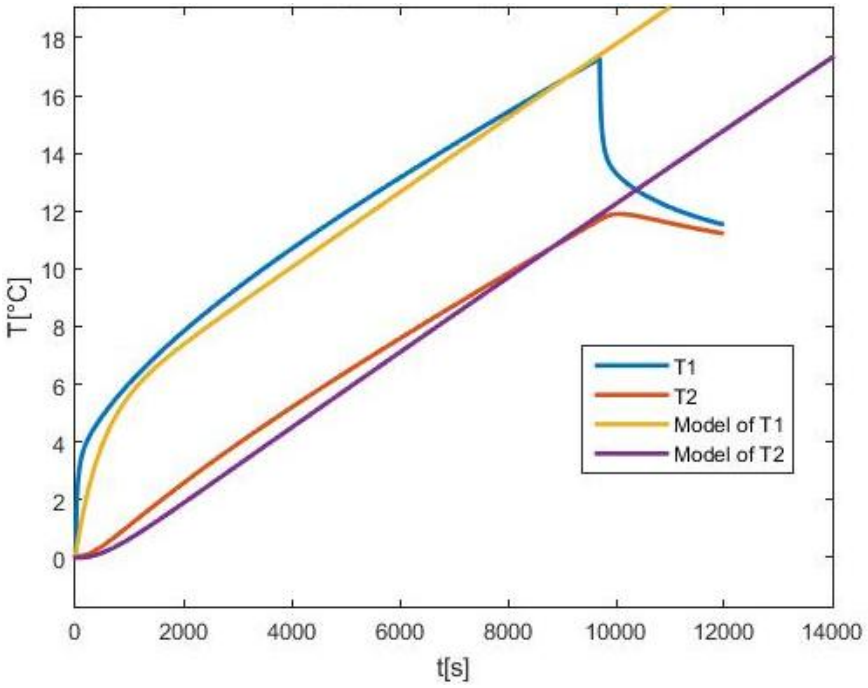

Fig. B. 5: Modeled temperatures fitted to measured temperatures T1 and T2 on MRW45-V3

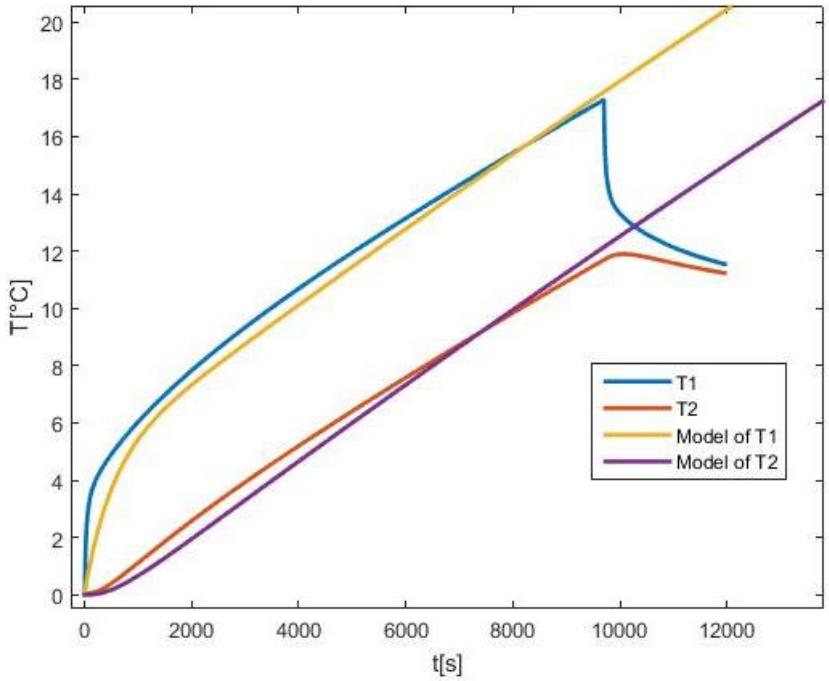

Fig. B 6: Modeled temperatures fitted to measured temperatures T1 and T2 on MRW55-V3

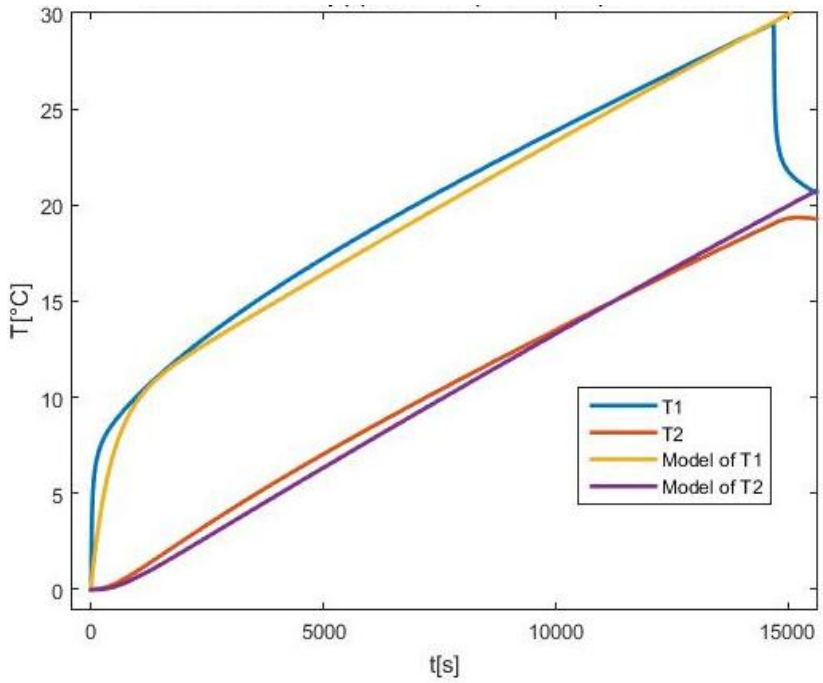

Fig. B.7: Modeled temperatures fitted to measured temperatures T1 and T2 on MRW65-V3

Appendix C: A script for evaluation of thermal contact resistance of contact of rolling elements in guideways

Values in this script correspond with setup of fit to temperatures measured on linear guideway SCHNEEBERGER BMW-V1.

```
clc
clear all
syms k1 f k m1 m2 m c1 c kn1 kt1 m11 m22 cn1 cs1 kn fre w t Qi kc real
nk=7;
qi=2; % node 3
ki=sym('ki',[nk,1]);
ci=sym('ci',[nk,1]);
K(k)=[k,-k;-k,k];
C(c)=[c,0;0,c];
Kg=blkdiag(K(ki(1)),K(ki(2)));
Cg=blkdiag(C(ci(1)),C(ci(2)));
for ii=3:nk
   Kg=blkdiag(Kg,K(ki(ii)));
   Cg=blkdiag(Cg,C(ci(ii)));
end
B=[];
for ii=1:nk-1
   B(ii,:)=[zeros(1,1+(ii-1)*2),1,-1,zeros(1,2*nk-3-(ii-1)*2)];
end
B=[B;
1,zeros(1,2*nk-1);
zeros(1,2*nk-1),1];
L=null(B,'r');
Ka=L'*Kg*L;
Ca=L'*Cg*L;
Q=sym(zeros(size(Ka,1),1));
Q(qi)=Qi;
A=1i*w*Ca+Ka;
tic;Ai=inv(A);toc;
% tic;Aif = matlabFunction(Ai,'file','Ai');toc
Qia=10;
A1=-inv(Ca)*Ka;
p1=8.50e6;
p2=1.0e0;
p3=0.9e0;
p4=1.4e0;
p5=4.5e0;
p6=p1;
p7=2e0;
```

```
p8=0.45e0;
p9=5.5e0;
p10=3.5e0;
ki4=1e0;
Ki=[1e-6*p1;0.0047295*p2;13.09*p3;ki4;8.387*p4;0.00473*p5;1e-6*p6];
Ci=[0;30.31*p7;569.234*p8;0;144.518*p9;30.31*p10;0];
A1=subs(A1,[ki,ci],[Ki,Ci]);
Q1=subs(Q,Qi,Qia);
Ca1=subs(Ca,ci,Ci);
tic;[V,D]=eig(A1);toc;
T=V*inv(D)*(expm(D*t)-eye(size(A1)))*inv(V)*inv(Ca1)*Q1;
tic;
T3s(t)=T(2);
T6s(t)=T(5);
digits(6)
toc;
ts=100;
vpa(T3s(ts))
vpa(T6s(ts))
ts=200;
vpa(T3s(ts))
vpa(T6s(ts))
ts=1000;
vpa(T3s(ts))
vpa(T6s(ts))
ts=3000;
vpa(T3s(ts))
vpa(T6s(ts))
ts=6000;
vpa(T3s(ts))
vpa(T6s(ts))
figure
plot(tv,T1v, tv, T2v)
hold on
ezplot(T3s,[0,6e3]);hold on
ezplot(T6s,[0,6e3])
```